NSWC TR 87-342

YTTERBIUM GAUGE MEASUREMENTS TO OBTAIN STRESS-TIME PROFILES IN SHOCKED CAST COMPOSITION B-3

BY GERRIT T. SUTHERLAND

RESEARCH AND TECHNOLOGY DEPARTMENT

APRIL 1989

NAVAL SURFACE WARFARE CENTER

Dahlgren, Virginia 22448-5000 • Silver Spring, Maryland 20903-5000

REPORT DOCUMENTATION PAGE

1a. REPORT SECURITY CLASSIFICATION UNCLASSIFIED	1b. RESTRICTIVE MARKINGS
2a. SECURITY CLASSIFICATION AUTHORITY	3. DISTRIBUTION/AVAILABILITY OF REPORT Approved for public release; distribution is unlimited.
2b. DECLASSIFICATION/DOWNGRADING SCHEDULE	
4. PERFORMING ORGANIZATION REPORT NUMBER(S) NSWC TR 87-342	5. MONITORING ORGANIZATION REPORT NUMBER(S)
6a. NAME OF PERFORMING ORGANIZATION Naval Surface Warfare Center 6b. OFFICE SYMBOL (If applicable) Code R13	7a. NAME OF MONITORING ORGANIZATION Office of Naval Technology, ONT-23
6c. ADDRESS (City, State, and ZIP Code) 10901 New Hampshire Avenue Silver Spring, MD 20903-5000	7b. ADDRESS (City, State, and ZIP Code) Washington, D.C. 20362
8a. NAME OF FUNDING SPONSORING ORGANIZATION 8b. OFFICE SYMBOL (If applicable)	9. PROCUREMENT INSTRUMENT IDENTIFICATION NUMBER
8c. ADDRESS (City, State, and ZIP Code)	10. SOURCE OF FUNDING NOS PROGRAM ELEMENT NO.: PE62314N PROJECT NO.: NS3A TASK NO.: RJ14E31 WORK UNIT NO.: 9R4TBK
11. TITLE (Include Security Classification) Ytterbium Gauge Measurements to Obtain Stress-Time Profiles in Shocked Cast Composition B-3	
12. PERSONAL AUTHOR(S) Sutherland, Gerrit T.	
13a. TYPE OF REPORT 13b. TIME COVERED FROM TO	14. DATE OF REPORT (Yr., Mo., Day) 1989, April 15. PAGE COUNT 90
16. SUPPLEMENTARY NOTATION	

17 COSATI CODES			18. SUBJECT TERMS (Continue on reverse if necessary and identify by block number)
FIELD	GROUP	SUB-GR	Shockwaves, Ytterbium Piezoresistant, Composition B-3 (JLS)
42	01		
20	11		

19. ABSTRACT (Continue on reverse if necessary and identify by block number)

Ytterbium gauges were successfully used to measure stress-time profiles in cast Composition B-3. Targets of Composition B-3 containing one or two imbedded ytterbium gauges were impacted with either a fused silica or a Composition B-3 flyer. This report demonstrates that symmetric impact loading and unloading gas gun experiments using Composition B-3 can be performed.

Peak stresses measured were compared with results of a previous study using quartz gauges [J. Appl. Phys., Vol. 58, No 6256, 1983]. Stresses were obtained with the aid of an inclusion analysis [J. Appl. Phys., Vol. 53, No. 6256, 1983]. Peak stresses obtained were not in the stated accuracy of predicted stress values (based on the above study) when inclusion analysis used parameters obtained from calibration experiments performed for this study. However, peak stresses were within the stated accuracy of predicted (continued)

20. DISTRIBUTION/AVAILABILITY OF ABSTRACT	21. ABSTRACT SECURITY CLASSIFICATION
___ UNCLASSIFIED UNLIMITED X SAME AS RPT ___ DTIC USERS	UNCLASSIFIED

22a. NAME OF RESPONSIBLE INDIVIDUAL	22b. TELEPHONE NUMBER (Include Area Code)	22c. OFFICE SYMBOL
Gerrit T. Sutherland	(301)394-1406	Code R13

Block 19. (continued)

stress values when the inclusion analysis used parameters obtained from Gupta and Gupta [J. Appl. Phys., Vol. 61, 1987].

Calibration experiments and quasi-static experiments were performed to generate inclusion analysis parameters and constants. Experiments were performed in which a PMMA target was impacted with a thin PMMA flyer. In these experiments, the target was loaded to a peak longitudinal stress and then unloaded to zero longitudinal stress. Resistance measurements were recorded for both loading and unloading.

Suggestions for future work, and possible improvements in experimental design and techniques are presented.

FOREWORD

Much effort has been expended in characterizing the propagation of shock waves through explosives. Researchers modeling explosive behavior and explosive systems (warheads) need accurate constitutive relations to perform hydrocode calculations. These researchers require information on pressure ranges within an explosive which include: pressure ranges (0-20 kbar) described by the unreacted Hugoniot, pressure ranges (20-350 kbar) described by reactive flow (the onset of chemical reaction and leading to burning and detonation), and a pressure range (125-350 kbar) which encompasses fully reactive or detonation behavior. A primary goal of the Office of Naval Technology 6.2 Explosive Block Program is to characterize the explosive response of a prototype Navy plastic-bonded explosive (PBX). This report describes the preliminary work required to develop the technology to pursue this goal.

Dr. J. W. Forbes is acknowledged for his support, guidance, and intensive reviews of this manuscript. Messrs. A. D. Brown and R. N. Baker are thanked for their superior assistance in constructing the experiments. Mr. D. G. Tasker is thanked for his advice on electrical circuitry, data acquisition and computer programing. Ms. Wanda Morat is thanked for her editorial reviews of this report. Messrs. W. Watt and M. Savage are thanked for their advice on experimental apparatus. Mr. R. J. Lee is thanked for his assistance in performing some experiments. Mr. P. Gustavson is thanked for his help in modifying the ytterbium gauge power supply. Dr. E. R. Lemar is thanked for his advice on construction of experimental apparatus. Mr. M. Austin is thanked for his precise machining of explosive samples. Messrs. W. Freeman, J. Roscher and D. Ashwell are thanked for machining parts of the experimental apparatus.

I also acknowledge the generous assistance of Dr. Y. M. Gupta of the Shock Dynamics Laboratory of Washington State University. One batch of ytterbium foils was statically tested and one target was partially constructed at the Shock Dynamics Laboratory. Dr. N. S. Brar of the University of Dayton (formerly of Washington State University) is thanked for demonstrating static testing, and for his analysis and advice on experimental design and data analysis. Mr. J. T. Thompson of Washington State University is thanked for training Mr. R.N. Baker in the fabrication of gas gun targets and gauges. Mr. M. Wong is thanked for his advice on ytterbium quasi-static and dynamic calibration experiments.

This work was performed as part of the Explosives Project within the Office of Naval Technology Block Program for Explosives and Undersea Warheads.

Approved by:

KURT F. MUELLER, Head
Energetic Materials Division

CONTENTS

ILLUSTRATIONS

ILLUSTRATIONS (Cont.)

ILLUSTRATIONS (Cont.)

ILLUSTRATIONS (Cont.)

TABLES

CHAPTER 1

INTRODUCTION

Much effort has been expended in characterizing the propagation of shock waves through explosives. Researchers modeling explosive behavior and explosive systems (warheads) need accurate constitutive relations to perform hydrocode calculations. These researchers require information on pressure ranges within an explosive which include: pressure ranges (0-20 kbar) described by the unreacted Hugoniot, pressure ranges (20-350 kbar) described by reactive flow (the onset of chemical reaction and leading to burning and detonation), and a pressure range (125-350 kbar) which encompasses fully reactive or detonation behavior. A primary goal of the Office of Naval Technology 6.2 Explosive Block Program is to characterize the explosive response of a prototype Navy plastic-bonded explosive (PBX). This report describes the preliminary work required to develop the technology to pursue this goal.

Shock response characteristic Composition B-3, PBXN-110 (formerly PBXW-113), PBXW-109, and PBXW-114-II have been studied at NSWC by Lemar et al[1,2] by using a quartz gauge technique. The compositions of these explosives are given in Table 1. These experiments were designed to obtain unreacted Hugoniot measurements. Hugoniot determinations require the use of the Rankine Hugoniot jump conditions and measurement of two parameters (pressure, particle velocity, shock speed, volume, or energy). Lemar et al typically measured pressure and shock speed for a known projectile velocity.

Rankine Hugoniot jump conditions are only valid for steady waves; a steady wave is a wave whose profile in pressure-time space does not change as it propagates through a material. Quartz gauge measurements are an excellent technique for obtaining low pressure Hugoniots, if the steady wave condition is met.

Lemar et al's quartz gauge measurements revealed pressure-time profiles of PBXs which indicated unsteady wave behavior. The stress gradually increased after the initial shock in PBXN-110, PBXW-109, and PBXW-114; these behaviors may be due in part to a shock induced chemical reaction. These results indicate that measurement techniques that can determine unsteady flow properties are necessary to accurately characterize some Navy PBXs.

Nunziato et al[3] reported that, in the explosive PBX-9404, a stress increase or ramp was observed after the explosive was initially shocked. Additionally, the strength or magnitude of the initial shock front grew as this front propagated in the explosive. Nunziato et al developed a theoretical criteria to determine the onset of growth or decay at a shock front and growth after the shock front in an explosive. To fully characterize an explosive, the types of stress growth have to be determined and theoretical modeling has to be done. To study these unsteady wave behaviors, it is advantageous to

measure pressure-time profiles at various positions in the sample being shocked. Therefore, an insitu measurement technique would be best for investigating the role of kinetics on the shock response of explosives.

Many researchers[4,5,6] have used multiple manganin piezoresistive gauges to measure the shock and detonation wave response of explosives. Some researchers[7] have used multiple electromagnetic particle velocity (EMV) gauges to measure particle velocity-time profiles in explosives. Vorthman[8] et al developed a technique which employs multiple EMV and electromagnetic impulse gauges to measure particle velocity and stress profiles in an explosive. We will concentrate our efforts on piezoresistive gauges.

The low resistivity change per unit stress in manganin gauges prevented the use of these gauges for explosive stresses below 20 kbar. Therefore, ytterbium gauges were chosen for this study. Manganin gauges will be used in future experiments in which the explosive will be subjected to pressures above 20 kbar.

Ytterbium gauges are one of many piezoresistive gauges which also include manganin and carbon gauges. Bridgeman[9] first discovered the phenomena of piezoresistance in 1911. Bridgeman[10] used manganin gauges to measure stress in static experiments in 1958. Fuller and Price[11] first used manganin gauges in shock experiments in 1962. Ytterbium gauges were first developed by Keough.[12] Further studies of ytterbium gauges include Keough[13] and Ginsberg et al.[14] Additional work on characterizing and measuring the response of ytterbium gauges has been performed by Y. M. Gupta[15,16] and coworkers; his numerous publications are referred to throughout this report.

The goals of our study are to calibrate ytterbium gauges and develop methods for using them in an explosive. The ytterbium gauges should measure stress to an accuracy of ± 5 percent. Ytterbium gauges were traditionally calibrated empirically on loading; these calibrations will not accurately describe the unloading response because of gauge hysteresis. Gupta[15] has developed a continuum model which describes the resistance change of a ytterbium gauge as a function of stresses and strains in the gauge. Gupta[15] has also developed an inclusion analysis to determine the stresses and strains in the gauge as a function of stresses and strains in the material (matrix) surrounding the gauge. His main interest has been to predict the gauge response for a known matrix stress. Note that practical use of the gauge requires solving the reverse problem of finding the matrix stress from the resistance change of the gauge.

Gupta's continuum models require that calibration experiments be performed and that the ytterbium gauge material undergo tensile testing. The gauges are calibrated over a wide range of stresses and strains to allow their use in experiments with various stress-strain conditions. These experiments and testing will be described in this report. It was clearly demonstrated in the current work that to use the model by Gupta, the matrix surrounding the gauge must be elastic or plastic over the stress range of interest.

Experiments were performed using Composition B-3, and stress measurements are compared with those of Lemar[1] et al. Composition B-3 was used because it is a Navy composite explosive with an existing data base and it is easy to machine. Experimental techniques were learned when Composition B-3 targets were constructed; these techniques will allow us to perform experiments using targets of Navy PBXs.

CHAPTER 2

CALIBRATION EXPERIMENTS

This chapter describes the tensile testing and dynamic calibration experiments required to calibrate ytterbium gauges. It includes sections on: the PIEZORESISTIVE MODEL, TENSILE TESTING, and DYNAMIC CALIBRATION EXPERIMENTS.

PIEZORESISTIVE MODEL

The relative resistance change of a ytterbium gauge is related to the stresses and strains in the ytterbium[16] by Equation (1). Directions (see Figure 1) are: (1) along width of gauge, (2) along thickness of gauge, and (3) along length of gauge.

$$\frac{\Delta R}{R_o} = \pi_{12}(\Delta\sigma_1 + \Delta\sigma_2) + \pi_{11}\Delta\sigma_3 + \eta\Delta\gamma_p - \Delta\epsilon_1 - \Delta\epsilon_2 + \Delta\epsilon_3 \quad (1)$$

where:

ΔR = resistance change of gauge

R_0 = initial resistance of gauge

σ_i = stresses in the ytterbium gauge in kbar

ϵ_i = strains in the ytterbium gauge

γ_p = accumulated plastic strain in gauge

π_{1j} = piezoresistive coefficients

η = electrical strain hardening coefficient

The resistance of a ytterbium gauge is determined by three physical effects. The stress terms (products of elements of stress and piezoresistive tensors) in Equation (1) model the resistance change that occurs when the ytterbium metal is stressed (piezoresistance). The strain terms model

the resistance change caused by any dimensional change of the gauge. The term $\eta\Delta\gamma_p$ models the gauge resistance increase caused by defects produced in the ytterbium during plastic work on the gauge. These defects are produced during both plastic loading and unloading. The accumulated plastic strain (γ_p) is defined to be a scaler and will increase upon plastic loading and unloading.

To use Equation (1), the dependence of the stress and strain (our shock experiments are one dimensional in strain) existing in the target material on the stresses and strains in the gauge need to be determined. In this study we use an inclusion analysis computer code based on Gupta's inclusion analysis.[15] Some features of the inclusion analysis are discussed in Appendix A. For a given strain in the target material, the program calculates the stresses in the target material and the stresses, strains, and accumulated plastic strain in the ytterbium gauge. These values are then inserted into Equation (1) to find the gauge resistance.

Equation (1) requires values for the piezoresistive (π_{1j}) and electrical strain hardening coefficients (η). The static values of the piezoresistive coefficients are determined from tensile testing. These coefficients are pressure dependent. A simple model for pressure dependence of the piezoresistive coefficients is assumed to be adequate.[17] This model[18] is given by Equations (2) through (4).

$$\pi_{11} = \pi_{11}|_o + m\,p \tag{2}$$

$$\pi_{12} = \pi_{12}|_o + m\,p \tag{3}$$

where:

$$\text{pressure} \equiv p \equiv \frac{-\sigma_1 - \sigma_2 - \sigma_3}{3} \tag{4}$$

The statically measured piezoresistive coefficients are given by $\pi_{11}|_o$ and $\pi_{12}|_o$, their pressure dependence by a coefficient m. Dynamic calibration experiments were performed to determine m. These experiments also determined the electrical strain hardening coefficient (η) as a function of the accumulated plastic strain (γ_p).

As stated above, the inclusion analysis program calculates the stresses and strains in the gauge from the stresses and strain in the target material. In summary, this program requires the use of coefficients m and η, which are obtained from dynamic calibration experiments. Also, the program requires the coefficients $\pi_{1j}|_o$, yield strength of ytterbium, and the mechanical strain hardening of the ytterbium gauge material. These values are found from tensile testing. Other constants that are required in the inclusion analysis are the bulk and shear modulus of ytterbium gauge material. The bulk modulus of 148.0 kbar was found from hydrostatic testing at SRI International.[14,19] A shear modulus of 58.3 kbar was calculated[20] using the above bulk modulus value and measured mean Young's modulus value obtained from quasi-static testing.

TENSILE TESTING

Quasi-static (tensile) testing for the first batch of ytterbium foils was performed at Washington State University. Static testing and dynamic calibration experiments are required to characterize the ytterbium foils. Chen, Gupta, and Miles[21] developed the method to test the foils. Experimental equipment, methodology, and analysis are described in their journal article. Test samples were machined out of the ytterbium foil. These strips were machined to a configuration illustrated in Figure 2. These foils were pulled along the sample axis by use of a Terra-Tek Model 3292.2 test system. The foils were subjected to one dimensional stress along the length of the test samples. Stress, strain, and resistance of the foils were measured for loading, unloading, and reloading. Stress-strain paths during loading and unloading, and reloadings and unloadings during quasi-static testing, are shown in Figure 3.

Ytterbium foils were obtained from the Research Chemical Division of the Nucor Corporation of Phoenix, Arizona. Foils (batch Yb-M-3-218C) were obtained in the form of 3-inch x 3-inch squares approximately 0.002-inches thick. Thickness was obtained by measuring the area and weighing parts of each foil. Area was obtained by measuring lengths and widths of foil pieces with a Gaertner traveling microscope; mass was obtained using a Prescisa 200A electronic balance. Equation (5) was used to determine thickness; this method is consistent with the method used by Chen et al.[21] Table 2 lists the thickness determinations obtained. Note that a small error in density of the foil results in the same percentage error in thickness.

$$t = \frac{ms}{A\,\rho} \tag{5}$$

where:

A = area in cm^2

ρ = density in g cm^{-3}

ms = mass in g

t = average thickness

As mentioned previously, tensile testing provides values of the coefficients $\pi_{11}|_o$ and $\pi_{12}|_o$, ytterbium yield strength, ytterbium Young's modulus, and the mechanical strain hardening of ytterbium. The yield strength is taken as the point on the quasi-static loading stress-strain curve where the first deviation from perfectly elastic behavior occurs. The mechanical strain hardening (x_m) is the increase in stress per unit strain during plastic loading. No mechanical strain hardening was found during tensile testing and the mechanical strain hardening coefficient was taken

to be zero (the material was perfectly plastic). Measured material constant values from static testing are recorded in Table 3. Mean values and the standard deviation of these values are given in Table 4.

DYNAMIC CALIBRATION EXPERIMENTS

Dynamic resistance experiments and quasi-static tensile testing are required to find the pressure dependence (m) of the piezoresistive coefficients and the electrical strain hardening coefficient (η). To find these coefficients, dynamic resistance measurements are performed. Gauges are placed in a material (matrix) which is subjected to dynamic loading to a known longitudinal stress, and then unloaded to zero longitudinal stress. The resistance of the gauges is measured during both loading and unloading. The peak resistance measured upon loading is needed to calculate the pressure dependence (m) of the piezoresistive coefficients [Equations (2) through (4)]; the residual resistance measured upon unloading is needed to calculate the constant η.

Dynamic calibration experiments were performed using the NSWC 3.5-inch light gas gun facility located in Building 325. Experimental construction, experimental electronics, data acquisition, and piezoresistance constants determination will be discussed in the following sections of the chapter.

Experimental Construction

Calibration experiments (86-010, 87-002, and 87-003) were performed using symmetric impact loading-unloading experiments (Figure 4). In this experimental configuration, the particle velocity is one half the measured projectile velocity. These experiments were constructed out of type 2 Rohm & Hause UVA polymethyl methacrylate (PMMA). PMMA was chosen for a target and flyer material because it was easily obtainable and easily machinable. A maximum longitudinal stress of 9 kbar can be attained in this configuration; this stress limit results from the previous maximum projectile velocity of our gas gun (0.48 mm/μsec) and the low shock impedance of PMMA. Modifications have been performed to our gas gun to allow for a greater projectile velocity. To attain a higher peak stress, one experiment (S87-001) was performed in which a thick aluminum flyer impacted a PMMA target (see Figure 5).

The ytterbium gauges were machined out of the foil material to a configuration that is depicted in Figure 6. Copper foil leads were then soldered to the gauge. The gauges were placed between 2-inch diameter PMMA plates. Gauges were placed about 1 and 3 mm from the impact surface (Figure 4). Hysol epoxy, composed of RE2038 resin and HD3404 hardener, was used to fill the volume in the gap where there was no gauge (Figure 6). This PMMA sample was potted in an epoxy target which is illustrated in Figure 7. The trigger pins depicted in Figure 7 serve to trigger oscilloscopes and gauge power supplies. Impactor design is also illustrated in Figure 7.

In experiment S86-010, whose PMMA target was constructed at Washington State University, one gauge was placed in grooves machined in the PMMA (gauge 2) and the other gauge was placed between plates (gauge 1). The advantages and disadvantages of placing gauges in grooves are discussed in Chapter 4 of this report.

Experimental Electronics

The electrical circuit used to record the voltage drop across the inner gauge leads (Figure 6) is schematically depicted in Figure 8. This circuit is essentially the same circuit as that used by Gupta et al.[16] A slightly different circuit was used in experiment 86-010. In this experiment, the ballast resistors R3 and R4 were inadvertently placed parallel to the power supply output instead of in series.

The power supply (California Avionics #1520AR) supplies a constant current of 0-9 amps (depending on the load) to the current leads of each ytterbium gauge. This current duration can be adjusted to from 25 to 125 μsecs. Gauge signals are recorded with 7844 Tektronics and, in some cases, with 2090 Nicolet digital oscilloscopes. In a typical experiment, backup scopes were triggered along with the power supply; primary scopes were triggered shortly before the shockwave impinged on the gauges.

In experiments 87-003, 87-004, 87-008, and 87-009 the current going to one of the gauges was monitored with a #411 Pearson Coil. Output from the Pearson Coil (an isolated signal is obtained with a voltage proportional to the current flowing through the coil) was recorded with a 2090 Nicolet oscilloscope. This monitoring was to ascertain when there was constant current flowing through the gauge during the experiment.

Carbon resistors located in the filled epoxy targets of experiments 87-001 through 87-004 were used as ballast resistors (R3 and R4 in Figure 8). This epoxy is shocked at the same time as the sample. When the carbon resistors are shocked, they decrease in resistance and more current flows through the gauge. This increases the voltage drop measured across the active area of the gauge. Evidence of a late time gauge current increase was found in experiments 87-001 and 87-002. The residual resistance change upon unloading for experiment 87-002 could not be measured for gauge 2. A #411 Pearson current probe and a Nicolet 2090 oscilloscope were used to measure the current flowing from the power supply to the gauge in experiment 87-003. The Pearson coil record and profiles suggest that the resistors were shocked after the time of interest in experiment 87-003. Carbon resistors were located away from the target so that they would not be shocked in latter experiments (87-008 through 87-011).

Data Acquisition

Gauge records and time calibration records were obtained in the form of pictures of oscilloscope traces (oscillograms). The spatial coordinates of points on the traces were found using a Gaertner Toolmakers microscope (model M2001RS) and a digital display unit. These digital values were input into the data reduction computer program DREDUCE.[22] This program converts the spatial coordinates obtained from the microscope into voltage-time points and relative resistance-time points. Nicolet data was transferred to a Compaq 286 Deskpro computer with the aid of the computer program GNIC.[23] The use of Nicolet oscilloscopes is discussed in Appendix B.

The relative resistance change ($\Delta R/R_o$) was found from the measured voltage change ($\Delta V/V_o$) by an analysis by Wilkinson appearing in a report by Keough.[24] This correction amounts to about a 1 to 3 percent correction and is needed because the resistance of the ytterbium gauge leads [(R6 - R9) of Figure 8) change during the experiment. The gauge leads exit the sample; copper leads are connected to the ytterbium leads outside the sample. Only the parts of leads inside the sample were assumed to change resistance. For experiment 86-010, which used a slightly different circuit, the relative resistance change was found by a suitably modified circuit analysis.

Projectile velocity was measured using electrical shorting pins placed in the gun barrel near the target. Tabular data by Barker and Hollenback[25] for an "equilibrium" Hugoniot of PMMA was interpolated to find longitudinal stress in the PMMA for known particle velocities. PMMA is a viscoelastic material and does not exhibit steady wave material above 8 kbar; however, a steady stress value is obtained after the initial dispersive wavefront, and Barker terms Hugoniots using these values as "equilibrium" Hugoniots. Barker et al gave no functional form for this Hugoniot. Strain was also found by interpolating tabular data of Barker and Hollenback. The longitudinal stress for experiment 87-001 was found from known impedance matching techniques. Projectile velocities, particle velocities, and longitudinal stress are displayed in Table 5.

The measured peak and residual relative resistive change measurements appear in Table 6. Figures 9 through 12 show experimental relative resistance ($\Delta R/R_o$)-time profiles of the calibration experiments.

Piezoresistive Constants Determination

Two parameters needed by the inclusion analysis are found from the dynamic calibration experiments. The pressure coefficient m of the piezoresistive coefficients (π_{11}, π_{12}) and the constant η are obtained. The coefficient m adjusts the piezoresistive coefficients for pressure and is used in Equations (2) and (3). The coefficient η is defined by Gupta[18] as a scaler measure of the increase in gauge resistance due to defect production during plastic flow in the ytterbium matrix. To find these coefficients, many inclusion analyses are performed. Various values of m and η are used. For each value of m and η the inclusion analysis computer code will predict a peak and a residual resistance change. For each experiment values of m and η are determined such that the inclusion analysis code will predict experimentally measured peak and residual relative resistance changes.

The inclusion analysis will find the stresses and strains in the ytterbium from the stresses and strain in the matrix. These stresses and strains are then inserted in Equation (1) to find relative resistance changes. In experiments where gauges are placed in grooves machined in the target material, the matrix is taken to be the target material. In experiments where the gauges are placed between ("sandwiched") plates, the matrix is taken to consist of the target material and the glue surrounding the gauge sides (Figure 6). The ytterbium is assumed to be an elastic-plastic material while the matrix has to be either completely elastic or plastic. This is because the inclusion analysis has not been extended to treat elastic-plastic matrices.

The response on the matrix must be input into the inclusion analysis. In ungrooved gauge experiments (Figure 6), Hysol epoxy surrounds the gauge sides. In ungrooved gauge experiments,

the matrix (target material and glue) was specified by inputting a bulk and shear modulus into the inclusion analysis. A longitudinal modulus (L) was specified [Equation (6)] to match that of PMMA. This means that the longitudinal stress-strain relationship for the matrix will match that of PMMA. This path in stress-strain space is that of the Rayleigh line. A shear modulus is specified such that the shear modulus of the matrix is the same as the shear modulus of the glue. For an elastic matrix, the value inserted for shear modulus determines the magnitude of the shear or transverse stress components.

For an elastic matrix, a shear modulus (μ) for this epoxy was found from transverse sound velocity (C_t) measurements[26] [see Equation (7)] and was taken to be the shear modulus of the matrix. The inclusion analysis requires a bulk modulus that is found from Equation (6).

$$L = \frac{\sigma}{\epsilon} = K + \frac{4}{3}\mu \tag{6}$$

$$C_t^2 = \frac{\mu}{\rho_o} \tag{7}$$

where:

K = bulk modulus

μ = shear modulus

L = longitudinal modulus

ρ_o = initial density

σ = stress

C_t = transverse sound speed

ϵ = strain

For the grooved gauge, the shear modulus for PMMA was taken from inclusion analysis computer runs by Brar[27] as 23.70 kbar.

A hydrostatic analysis can be performed by finding the correct longitudinal modulus [see Equation (6)] for the PMMA and inputting a shear modulus that is very low (10^{-7} kbars). Numerical computational errors will occur in the inclusion analysis program if a zero shear modulus is used.

The results of inclusion analysis using both matrix assumptions are given in Tables 7 and 8. The results of experiment 87-001 were not used because: (1) it was a single shock compression experiment not a symmetric impact experiment, (2) the air bubble observed around gauge 1 could have influenced the records obtained from gauge 2, and (3) PMMA exhibits viscoelastic behavior above 8 kbar.

Figure 13 displays the product of the coefficient η and the accumulated plastic strain ($\Delta\gamma_p$) plotted as a function of the accumulated plastic strain for both the hydrostatic and elastic matrix assumptions. Figure 13 also displays data for the grooved experiment and experiments of Gupta and Gupta.[28] From the $\eta\Delta\gamma_p$ versus $\Delta\gamma_p$ plot a value for η can be found for a given value of $\Delta\gamma_p$. Figures such as Figure 13 will allow a value for η to be determined for explosive experiments; similar figures will also be used in Chapter 4 to look at the effect of various matrix assumptions on the determination of η. The product $\eta\Delta\gamma_p$ appears in Equation (1) and represents the relative resistance change in ytterbium due to defects produced when the ytterbium is plastically deformed.

As a test of the above analysis, the inclusion analysis parameters obtained above will be used to analyze calibration experiments. This program generates a table which, for a given relative gauge resistance, gives a corresponding matrix longitudinal stress. A computer program MATE[29] takes the above tables and experimental $\Delta R/R_o$-time records and generates stress-time profiles. In symmetric impact experiments, the exact stress upon loading and unloading (zero) is known. Variation from the true stresses can be found by inspection of Figures 14 through 17 and Table 9. The above profiles were generated using an inclusion analysis (elastic matrix assumption), meaning m was set to 1.24×10^{-3} kbar^{-2} (mean value); the coefficient η was found from inspection of Table 7. Table 9 gives an estimate on the variation to be expected in explosive experiments. This table indicates that one can expect a variation of $\pm$ 6 percent in stress measurements. A stress-time record for experiment 87-001 was also obtained; a stress 5 percent lower than the known stress was measured.

CHAPTER 3

EXPLOSIVE EXPERIMENTS

Ytterbium gauge experiments were performed to measure stress-time profiles in cast Composition B-3. Composition B-3 was chosen because experimental results could be compared with a recent study by Lemar et al,[1] it is an explosive which can be machined readily, and it is well suited to use with insitu gauges. The explosive was from the same batch as that used by Lemar et al. Gauges were placed between the explosive disks and then surrounded by a weak (low shear modulus) glue. Experimental construction, experimental electronics, data acquisition, and stress determination will be discussed in this chapter. An additional experiment was performed using pressed Composition B-3. This experiment will be discussed in a future publication.

EXPERIMENTAL CONSTRUCTION

Two experimental configurations (shown schematically in Figure 18) were used in the Composition B-3 experiments. The gauges where machined to the same dimensions as those used in the dynamic PMMA calibration experiments.

Configuration 1 has several features. Fused silica has a convex compression curve in pressure-volume space for pressures below about 25 kbar. Upon impact, a shockwave will be propagated into the explosive and a ramp wave into the fused silica; when this ramp wave reaches the back surface of the impactor, a partial release in the form of a rarefaction shock will be propagated back into the fused silica and on into the explosive. This means that the wave profile input into the explosive is well characterized.

Configuration 2 has several features. The carbon foam piece supports the Composition B-3 impactor to prevent it from bending and breaking during launch. Carbon foam has very low shock impedance; a release originating from the foam-Composition B-3 interface will allow the target to be unloaded to less than 2 kbar. The carbon foam allows a symmetric impact experiment; peak particle velocity will be one-half the projectile velocity. The greater rarefaction propagation distance (as compared to configuration 1) allows the release wave to be more dispersed for a particular sample depth.

The explosive targets were constructed using Eastman 910 glue ("Super Glue") to tack the gauges to the explosive sample. A glue similar to the binder used in PBXs was used to cement the explosive samples together. This glue consisted of one part dimeryl isocyanate (DDI 1410) to four parts hydroxyl-terminated polybutadiene resin (ARCO R45HT) with 0.097 percent dubyltin dilaurate catalyst. This glue was also used to pot the explosive samples into the targets.

EXPERIMENTAL ELECTRONICS

The electronic recording circuit is the same as that described in the dynamic calibration section in Chapter 2. The recording circuit was modified for improved performance by Tasker and Lee.[30] This supply will be used in future experiments; power supply modifications will be discussed in a future publication. In experiments 87-008 and 87-009 the 50 ohm ballast resistors were of a coaxial design by Tasker,[31] and were located approximately 1 meter from the target. The ballast resistance (resistors R3 and R4 in Figure 8) was increased from 20 to 50 ohms to reduce the correction required to convert the $\Delta V/V_o$ measurements into $\Delta R/R_o$ values. In addition, these shots were constructed so that no coaxial cable would be shocked.

DATA ACQUISITION

The data acquisition techniques employed to analyze explosive experiments are the same as those described in Chapter 2. A non-constant gauge current observed before the onset of the release in experiment 87-004 was detected by the current monitor. The voltage obtained from this experiment was corrected such that it would correspond to a constant gauge current.

EXPERIMENTAL MEASUREMENTS

Projectile velocities appear in Table 10. These velocities were measured by a series of electrical velocity pins placed in front of the target (see Figure 7). Explosive disk thicknesses were measured with a micrometer and appear in Table 11.

STRESS DETERMINATION

Inclusion parameters derived from the dynamic calibration experiments and quasi-static testing were incorporated into the inclusion analysis. This inclusion analysis was used to find stress-time profiles in the explosive from relative resistance change-time profiles. As with the ungrooved calibration experiments, the matrix was composed of the target and the glue which surrounds the gauge sides. The glue cures to a weak "rubber like state"; the shear modulus was taken to 1 kbar. A longitudinal modulus [see Equation (6)] was found by using the Hugoniot Data for Composition B-3,[1] and the Rankine Hugoniot jump condition as given below.

$$\epsilon = \frac{u_p}{U} \tag{8}$$

$$U = 3.0\ u_p\ ;\ u_p \leq .02675 \text{ mm } \mu\text{sec}^{-1} \tag{9}$$

$$U = 2.216 + 2.466\ u_p \tag{10}$$

$$\Delta\sigma = \rho_o\ U\ \Delta u_p \tag{11}$$

where:

σ = stress

ρ_o = initial explosive density

U = Lagrangian shock speed

u_p = particle velocity

The explosive experiments were analyzed with two sets of the coefficients m and η. One set was from the current calibration experiments, another from experiments by Gupta and Gupta.[28] Inclusion parameters used to analyze the explosive experiments are given in Table 12. The choice of inclusion parameters requires a detailed discussion which appears in Chapter 4.

For a given experiment the coefficient η must be known; the procedure for finding this coefficient is given below. An inclusion analysis (using a predicted stress) is performed to find the approximate plastic strain ($\Delta\gamma_p$) expected to occur in the explosive experiment. Figures 19 and 20 are then used to find the product $\eta\Delta\gamma_p$ for a given $\Delta\gamma_p$; the value of η can be found by dividing the resulting product by $\Delta\gamma_p$. Figures 19 and 20 display some of the information presented in Figure 13. Figure 19 displays a cubic spline fit of $\Delta\gamma_p$ versus $\eta\Delta\gamma_p$ for experiments of this study; Figure 20 displays a cubic spline fit for experiments of Gupta and Gupta.[28] The fitted function is not based on any physical assumptions. In Figure 19, the results of experiment 87-003 were averaged to produce a smooth spline fit.

Stress-time plots for all experiments performed are shown in Figures 21 through 28. Figures 21 through 23 display stress-time profiles generated with the use of an inclusion analysis in which parameters m and n were determined from an inclusion analysis (elastic matrix assumption) of calibration experiments. Note that the inclusion analysis of the explosive experiments is approximately hydrostatic. Figures 24 through 26 display stress-time profiles generated with the use of an inclusion analysis which used parameters m and η from a study of Gupta and Gupta.[28] Stress-time profiles from WONDY hydrocode runs are shown for comparison in Figures 21, 22, 24 and 25. A perfectly elastic-plastic model with Equations (8) through (10) was used in the hydrocode calculations. These hydrocode calculations are described in Appendix C. Figures 27 and 28 are generated with the same inclusion analysis as Figures 22 and 23; the profiles were measured using a

Nicolet oscilloscope instead of an analog scope. These profiles are displayed to show the results of using such an oscilloscope in these experiments. Further discussion on the use of Nicolet records is given in Appendix B.

Peak stresses and peak stress deviations from predicted values appear in Tables 13 and 14. Some of these deviations are shown graphically in Figures 23 and 26. Table 13 displays measured stresses obtained with coefficients m and η obtained from the dynamic calibration experiments; Table 14 displays measured stresses obtained with coefficients obtained from calibration experiments performed by Gupta and Gupta.[28]

Experiments 87-009 and 88-003 were constructed as multiple gauge experiments (configuration 2). In these multiple gauge experiments stress was measured in two places and shock velocities obtained. Gauges were nominally 2 and 6 mm deep (see Table 11) for experiment 87-009, and nominally 2 and 5 mm deep for experiment 88-003. Peak stress (see Tables 13 and 14) can also be obtained from the Lagrangian Rankine Hugoniot Jump condition (conservation of momentum) which is given by Equation (11). This method for obtaining stress is referred to as method 2 in Chapter 4.

A peak stress for the plastic wave for each experiment is obtained in Equation (11) from experimentally measured density, shock velocity, and a particle velocity. The stress and particle velocity at the Hugoniot Elastic Limit (HEL) were taken from Lemar et al[1] to be 1.4 kbar and 0.0272 mm/μsec.

The sound speed upon release was measured for experiments 87-009 and 88-003. Lagrangian sound speeds were measured and appear in Table 15. By a method described in Appendix D, these Lagrangian sound speeds were converted to Eulerian velocities. *Compression* (ρ/ρ_o) was found from manipulation of Rankine-Hugoniot jump conditions and a known particle velocity, and a calculated shock velocity [see Equation (10)].

CHAPTER 4

DISCUSSION

This chapter presents a discussion of results from the dynamic calibration experiments and information gathered from explosive experiments.

DYNAMIC CALIBRATION EXPERIMENTS

This section presents the advantages and disadvantages of placing gauges in grooves and also explores the assumptions used to analyze ungrooved gauge results. These experiments are required to find certain constants required in the inclusion analysis. The inclusion analysis is needed to find the stresses and strains in the gauge from the stresses and strains in the matrix. Once these stresses and strains are known, longitudinal stresses can be found from Equation (1) and experimental resistance measurements. The implications of dynamic calibration experimental results to the analysis of explosive experiments will also be discussed.

Grooved/Ungrooved Gauge Considerations

Ytterbium gauges have been placed in grooves in PMMA, fused silica, and in polycrystalline sapphire targets (matrices) by Y. M. Gupta and coworkers.[16,18,28] The reason for placing gauges in grooves is that this configuration best meets the assumptions of Gupta's inclusion analysis. The gauges are placed in grooves milled to high precision. The material surrounding the gauge is the same as that of the matrix. If the material is elastic (PMMA is elastic to 8 kbar, fused silica and the sapphire are elastic to about 70 kbar) the results can be analyzed with Gupta's inclusion analysis. Considerable machining time and skill are required to construct the grooves (especially in hard materials). The milling of precision grooves in most Navy explosives would be very difficult if not impossible. Precision grooves can not be cut into the explosives due to particle size and grain structure considerations.

The main advantage of the ungrooved or "sandwiched" gauge is the ease of experimental construction. As stated above, this configuration is the only feasible method in which to implement gauges in an explosive. To analyze the gauge response, the cured glue surrounding the gauge should be closely matched in material properties to that of the matrix and it should have a

hydrostatic response. Gupta et al[32] have successfully analyzed the response of ytterbium gauges in a hydrostatic medium (liquid CS_2). At present, the inclusion analysis used to find stresses from experimental resistance change records require that the matrix be either elastic or hydrostatic.

In experiment 86-010, a grooved gauge (gauge two) and an ungrooved gauge (gauge one) were placed in the same PMMA target. Measurements for the ungrooved gauge recorded a larger peak relative resistance change in addition to a larger relative resistance change than measured for the grooved gauge. The two gauges may have been machined from different foils. Other possible reasons the ungrooved gauge responds differently than the grooved gauge are discussed below.

Ungrooved Gauge Assumptions

Hysol epoxy (RE2038, HD3404) was used to fill gaps between plates in the PMMA calibration experiments. Hence, this glue was in contact with the ytterbium gauge sides. This glue is similar to EPON 815 (T1 Hardener) epoxy. EPON 815 is used extensively in shock experiments, and the Hysol epoxy was assumed to have the same shock response. The shock impedance of Epon 815 is very close to that of PMMA. Longitudinal and transverse sound speeds have been measured[33] for EPON 815 epoxy which suggests an initial elastic behavior. The shear moduli of PMMA and EPON 815 are also very close to each other. The above statements indicate that PMMA and EPON 815 should exhibit the same material response during elastic loading and unloading. This means that grooved and ungrooved PMMA experiments should give identical results if both the EPON 815 and PMMA remain elastic over the pressure range of the experiment (PMMA stays elastic to about 8 kbar).

The tensile strength of Hysol epoxy was given by the manufacturer as 9000 psi, assuming that the yield to occur during tensile failure means a yield strength of about 0.616 kbar. A Hugoniot Elastic Limit (HEL) of about 1.33 kbar would then be expected. The yield strength and HEL may vary with glue curing conditions, and may be different for a thin layer (0.05 mm) than for a thick bulk sample.

The yielding of the epoxy at a lower strength than that of PMMA suggests that an inclusion analysis which can treat an elastic-plastic matrix be used. Unfortunately, such an inclusion analysis does not exist.

The inclusion analysis calculates the transverse stress in a gauge (which is elastic-plastic) from the transverse stress in the matrix. The extent of coupling of transverse stresses present in the PMMA to the transverse stress existing in the epoxy is not treated in the inclusion analysis.

To analyze these experiments, the matrix is treated as either elastic or hydrostatic. Both assumptions result in some error in the inclusion analysis parameters obtained for this experimental configuration because the glue is an elastic-plastic material. The most reasonable set of inclusion analysis parameters will be determined for analyzing explosive experiments. The choice of the most reasonable will be discussed in the EXPLOSIVES EXPERIMENTS section below.

As discussed in the Dynamic Calibration Experiments section of Chapter 2, the results of calibration experiments are used to find two piezoresistive constants: the pressure coefficient of the piezoresistive coefficients (m) and the electrical strain hardening coefficient (η). The coefficients m and η are both determined by residual and peak relative resistance measurements; however, normally the coefficient m is strongly determined by the peak measurement, whereas the constant η is strongly determined by the residual measurement of relative resistance. The values for the pressure coefficient of the piezoresistive coefficients is displayed in Tables 7 and 8 for both matrix assumptions.

A mean value for the piezoresistive constants (see Chapter 2) $[\pi_{11}|_o, \pi_{12}|_o]$ was used in the inclusion analysis to find m. These constants varied between each foil and are expected to vary from region to region in each foil. This variation will cause a variation in the coefficient m. No attempt was made to use individual foil values of the piezoresistive coefficients for two reasons: (1) the piezoresistive coefficient for various regions of each individual foil were expected to vary, and (2) the gauges used in experiment 86-010 were constructed from an unknown foil. The coefficient m is an empirical constant and is not physically modeled at this time.

Determination of Coefficients m and η

The coefficients m and η were found both from a study by Gupta and Gupta[28] and by this study. Gauges were placed in grooves in a PMMA matrix. PMMA remains elastic to about 8 kbar; hence, the constants m and η were found from an *elastic matrix assumption. Experiments* of this study were modeled by both a hydrostatic and an eleastic matrix assumption.

Experiments Performed Elsewhere. Gupta and Gupta measured a pressure coefficient (m) of 7.6×10^{-4} kbar^{-2}. The value that is stated by Gupta and Gupta in Reference 28 is a misprint (7.6×10^{-3} kbar^{-2}).[17] Their constant determination is based on more experiments than were performed for this report. Coefficients (m) were measured from 6.0×10^{-4} to 1.1×10^{-3} kbar^{-2}.

The product $\eta\Delta\gamma_p$ from their experiments appears in Figures 13 and 20. Figure 20 shows the above product as a smooth monotonically increasing function of $\Delta\gamma_p$.

Elastic Matrix Assumption for Experiments of this Study. A mean pressure coefficient (m) of 1.24×10^{-3} kbar^{-2} was obtained. As can be seen from Table 7 values of m from 1.01×10^{-3} to 1.5×10^{-3} kbar^{-2} were measured. The mean measured value is considerably higher than that of Gupta and Gupta above. The use of the above mean value to analyze explosive experiments would result in lower stresses than stresses predicted with a m value of 7.6×10^{-4}. The magnitude of this effect will increase as the peak stress increases; this is discussed in this chapter.

Figure 19 shows the product $\eta\Delta\gamma_p$ again as a smooth monotonically increasing function of $\Delta\gamma_p$. Also the values of $\eta\Delta\gamma_p$ lie close to those measured by Gupta and Gupta.[28]

Hydrostatic Matrix Assumption for Experiments of this Study. As stated above, the glue used in calibration experiments did have strength (a yield of about 0.6 kbar). When the matrix is compressed and unloaded the matrix will respond both plastically and elastically. The stress region that the matrix responds plastically and the validity of the hydrostatic matrix assumption should increase as the peak pressures is increased above the yield point of the glue. In experiments of this study, a good part of the matrix response is elastic; hence, the above assumption is expected not to be valid. However, the hydrostatic matrix assumption results are given here for completeness.

The mean value for m obtained from the hydrostatic matrix assumption was 5.4×10^{-4} kbar^{-2}. For experiment 87-003, low values of m were obtained. These low values are the result of the high values of η needed to model the residual relative resistance change.

Figure 13 reveals that, for the hydrostatic matrix assumption, the product $\eta\Delta\gamma_p$ is large for small values of $\Delta\gamma_p$. This behavior is widely different than that measured by Gupta and Gupta (elastic matrix assumption).[28] Equation (1) reveals that the product $\eta\Delta\gamma_p$ represents the relative resistance change due to defects produced in ytterbium when the gauge is deformed. Therefore, the values of $\eta\Delta\gamma_p$ for the hydrostatic matrix assumption are physically unreasonable.

Grooved Gauge Experiment. One experiment was performed (experiment 86-010) in which a grooved and a ungrooved gauge were placed in PMMA. The grooved gauge was placed in PMMA which was elastic to about 8 kilobar; the gauge was in an elastic medium. An m value of 9.7×10^{-4} kbar^{-2} was obtained for this experiment. A low value of $\eta\Delta\gamma_p$ was obtained; more grooved gauge experiments would have to be performed to determine if this low value is due to a material property of the ytterbium, or due to a possible effect of the gauge not being perfectly surrounded by the groove.

Ytterbium Anisotropy/Ytterbium Foil Uniformity

A very recent observation has been the difference of response of the gauges when they are cut out of different orientations of each foil. These orientations are shown in Figure 29. Private communication with Wong[34] and Decarli[35] indicate that the Young's modulus and piezoresistive coefficients $\pi_{1j}|_o$ determined from pull testing are different when tensile test samples are cut perpendicular (C) rather than parallel (A) [see Figure 29] to the apparent grain of the foil. Wong[35] further observed in a dynamic calibration experiment in which two ytterbium gauges were cut out of different orientations [(B) and (D) of Figure 29] that the gauge response was substantially different (peak $\Delta R/R_o$ of 1.44 and 1.27 were measured). Wong suggests obtaining pull test samples for each direction of each foil and determining piezoresistive coefficients for each direction. The piezoresistive coefficients to be used in an inclusion analysis are those corresponding to the direction which is parallel to the length of pull test sample, and the length of the active area of gauge. The apparent grain direction was not noted for gauges and pull test samples fabricated for this study. It is also unknown whether this anisotropy existed for the ytterbium foils used in this study. This anisotropy could have been responsible for some of the variation observed in the response of gauges in this study. The piezoresistive model used by Gupta[15] assumes that the gauge material is isotropic. To completely physically model the response of ytterbium an anisotropic inclusion analysis needs to be developed.

From each ytterbium foil a pull test sample and several gauges were machined. It is assumed that the material properties of the test sample are the same as those of the foil. To test this assumption, several test samples would have to be tested from each foil. In this study, only one test sample was used per foil.

Dynamic Calibration Experiment Improvements

Two options for improved calibration experiments are available. One option is to use a very weak (hydrostatic) glue in calibration experiments. An inclusion analysis using the hydrostatic matrix assumption could then be used to find the required piezoresistive constants. The second option is to place the gauges in grooves in an elastic material. An inclusion analysis using the elastic matrix assumption would yield accurate piezoresistive constants. One or both of the above options will be used to find constants required to analyze future explosive experiments. Future grooved gauge calibration experiments should be performed using materials that stay elastic to above 20 kbar (i.e., fused silica) so gauges are calibrated over their measurement range (0-20 kbar).

Ytterbium gauges and tensile test samples should be cut in such a way that the sensing or active area of ytterbium gauges and length of the tensile test samples are parallel [i.e., (A) and (B) of Figure 29].

In a grooved gauge calibration experiment, the gauge is placed in an elastic matrix; the gauge will experience more accumulated plastic strain ($\Delta\gamma_p$) for a given longitudinal stress in an elastic matrix than in a hydrostatic matrix. In explosive experiments, gauges will be placed in explosives which will exhibit a hydrostatic matrix response. Using grooved calibration experiments means that the constant η will be determined for larger $\Delta\gamma_p$ than exists in explosive experiments.

If variation in gauge response of about 6 percent continues to be observed in future experiments, Lagrange analysis should be performed with caution. An error analysis as described by Cagnoux et al,[36] for example, should be performed to ascertain the spread in derived quantities (particle velocity, stress-strain paths, etc.) obtained from any Lagrange analysis procedure.

The variation in gauge response can be minimized. Gupta[37] states that a variation of $\pm$ 3 percent can be expected. To attain these results Gupta suggests grooved gauge dynamic calibration experiments should be performed. These experiments should be placed in an elastic matrix (fused silica) over the measurement range of the gauge.

EXPLOSIVE EXPERIMENTS

In this section, stress measurements and sound speed upon release measurements are discussed. Observations gathered from the experimental profiles obtained are documented.

Choice of Coefficients m and η

Unfortunately, the epoxy glue used in calibration experiments is chemically incompatible with explosives. The glue used in the calibration experiments was elastic-plastic; the polyurethane glue used in the explosive experiments was hydrostatic. Because of this glue difference, the coefficients m and η determined in calibration experiments (using the epoxy glue) may not be proper to use in explosive experiments. The coefficients, however, would be proper to use in experiments in which the epoxy was used.

There are three options for choice of the coefficients m and η: (1) use m and η found from dynamic calibration experiments and the elastic matrix assumption, (2) use m and η found from calibration experiments and the hydrostatic matrix assumption, and (3) use m and η found from experiments from Gupta and Gupta.[28] These choices will be discussed below. The peak stress obtained from each of the chosen assumptions will be discussed later in this chapter. The behavior of the above matrix assumptions is discussed earlier in this chapter. The effect of ytterbium anisotropy is not known. This effect could also cause differences between explosive experiments and calibration experiments if gauges for each type of experiment were cut in different orientations. It is assumed, but not known, that gauges from calibration experiments and explosive experiments were cut in the same direction.

Elastic Matrix Assumption. Explosive experiments will be analyzed with the coefficients determined from these experiments. The mean value for m will be 1.24×10^{-3} $kbar^{-2}$ and η will be found using Figure 19.

Hydrostatic Matrix Assumption. Explosive experiments will not be analyzed with m and η determined from calibration experiments which involved the use of a hydrostatic matrix assumption. These coefficients were not used for the following reasons. There is difficulty (see previous subsection Ungrooved Gauge Assumptions, Hydrostatic Matrix Assumption) in determining the proper value of m to choose (5.4×10^{-4} versus 7.7×10^{-4} $kbar^{-2}$). As discussed earlier in this chapter, the behavior of the product $\eta\Delta\gamma_p$ is unphysical. For low amounts of plastic strain in the ytterbium, very large η coefficients are indicated.

Coefficients from Experiments of Gupta and Gupta. Explosive experiments will be analyzed with those of Gupta and Gupta.[28] The key assumption here is that the value of m and η do not vary significantly from one ytterbium foil to another or one ytterbium foil batch to another. If this assumption is correct than the coefficients m and η should be more accurately determined in experiments of Gupta and Gupta because (1) they perform a number of experiments to determine m and η and (2) they perform grooved gauge experiments so that the matrix assumption is known.

Wave Profile Observations

The methods used and locations of stress-time profiles appear in Chapter 3 so they will not be given here. Experimental stress-time profiles (Figures 24 and 25) for experiments 87-004 and 87-008

reveal a dispersive elastic wave followed by a plastic wave. The time difference observed between the onset of the plastic wave and the onset of the release are in good agreement with the measured profile. The "bending" of the plastic wave at about 5 kbar may indicate viscoelastic behavior. This "bending" is similar to that observed for PMMA[25] which is known to be viscoelastic. The hydrocode model was not expected to reproduce the release wave shape because of its simplicity. It does reproduce the general features of the wave profile fairly well. In particular, future modeling will require a more complicated constitutive relationship for Composition B-3.

Experimental stress-time profiles for experiment 88-003 show again that a dispersive elastic wave is found, followed by a plastic wave. There is more bending in the plastic wave recorded by gauge 2 than by gauge 1. This observation supports the hypothesis of viscoelastic behavior.

Stress Measurements

Peak stress was calculated by two methods. Method 1 used a piezoresistive model and inclusion analysis of Gupta to find stress values from measured resistance changes. Two sets of the inclusion parameters m and η will be used: one set will be those derived from my dynamic calibration experiments (method 1a), and one set will be those obtained by Gupta (method 1b). Method 2 used the Rankine Hugoniot momentum jump condition (Lagrangian), and measured Lagrangian shock and projectile velocities to calculate a peak stress. In experiment 87-009, a shock velocity was measured and peak stresses could be calculated by method 2. This procedure is discussed in Chapter 3. These values were compared to stresses predicted with the use of Equation (10). Peak stresses and the difference in percent from predicted values are displayed in Tables 13 and 14.

Stresses measured using an inclusion analysis using constants derived from the present calibration experiments (method 1a) were not within the stated accuracy (± 5 percent) of the predicted results. The difference between predicted and measured (method 1a) appears to be due to inaccuracies in constants m and η as determined from the dynamic calibration experiments. The stresses measured using method 1b are generally (except experiment 87-009, gauge 2) within the stated accuracy of the calculated results. The results of the explosive experiment show that the constants determined from method 1b are more accurate than those determined from method 1a.

In addition, peak stress was calculated for experiment 87-009 by method 2. The peak stress determined in experiment 87-009 by method 2 is in excellent agreement with the predicted value.

As stated above, a dispersive elastic wave was found. It is hard to determine a HEL directly from the profiles. The HEL is the point on the pressure-volume surface of the Hugoniot which corresponds to plastic yielding of a material. HELs observed from inspection of the experimental profiles are consistent with HELs (1.06 - 1.95 kbar) measured by Lemar et al.[1]

Release Measurements

The Lagrangian sound speed upon release was obtained for experiment 87-009. The method used to obtain an Eulerian sound speed from the measured Lagrangian sound speed is described in Appendix C. A Lagrangian speed of 3.54 mm/μsec or an Eulerian sound speed of 3.30 mm/μsec was obtained for experiment 87-009. This value is higher than the measured elastic shock velocity of 3.14 mm/μsec. The elastic wave is unsteady (the wave shape changes with distance); different parts of the elastic wave will travel faster than others. Because the elastic wave did not have one unique elastic shock velocity, comparisons between sound speeds upon release and elastic shock velocities would be inappropriate.

The simple material model [Equations (9) and (10)] models Composition B-3 as a perfectly elastic-plastic material. In addition, the material is linearly elastic. This model assumption would then mean that the elastic wave speed would be constant at 3.00 mm μsec^{-1}. A higher speed measured for sound speed upon release from peak pressure than the elastic wave speed indicates that the elastic wave speed may be pressure dependent.

CHAPTER 5

CONCLUSIONS

Ytterbium gauges were successfully used to measure stress-time profiles in cast Composition B-3. The profiles were measured with either one or two ytterbium gauges embedded in cast Composition B-3 targets. Experiment 87-009 demonstrated that symmetric impact loading and unloading using explosives can be done. A dispersive elastic wave, a steady plastic wave, and a release are all evident in the stress-time profiles obtained. Experimental techniques were acquired and used to perform symmetric impact loading and unloading experiments. The stress-time records of gauges 1 and 2 in experiment 87-009 allowed observation of an evolving waveform. These gauges will allow the Navy to measure stress for long times (over 3 microseconds) at multiple locations. This technology will be applied to looking at unsteady wave behavior observed in Navy PBXs. Many of the techniques learned can be applied to future programs to measure the shock to detonation transition (SDT) by using manganin gauge technology.

Peak stresses measured using the ytterbium gauges, and using certain constants derived from the accompanying dynamic calibration experiments, were not within the stated accuracy of predictions based on a study of Lemar et al.[1] Peak stresses measured by the ytterbium gauges, using certain coefficients derived from dynamic calibration experiments of Gupta and Gupta,[28] were generally within the stated accuracy of the predicted stress value. In addition, excellent agreement existed between peak stresses calculated from measured shock velocities and stresses predicted based on a study of Lemar et al.[1]

The Composition B-3 experiments were very difficult to construct. Placement of gauges in a target without cracking the explosive plates, "bowing" the explosive plates, or forming a thick glue bond, was extremely difficult. These gauges should not be used on brittle materials. Navy PBXs (e.g., PBXN-110, PBXW-114, and PBXW-109) are "rubbery" or pliable; these explosive plates are not expected to crack or bow. In addition, these explosives have a very low shear modulus and hence behave almost hydrostatically (as a fluid).

Calibration experiments and quasi-static experiments were performed to generate inclusion analysis parameters and constants. Three shock experiments were performed in which a PMMA target was impacted with a thin PMMA flyer. In these experiments, the target was loaded to a peak longitudinal stress and then unloaded to zero longitudinal stress. Resistance measurements were performed for both loading and unloading. An inclusion analysis determined the coefficients m and η using an assumption that the matrix surrounding the gauges was elastic. When these coefficients were used to find peak stresses in explosive experiments, the stresses measured were not within the stated accuracy ($\pm$ 5 percent) of values predicted based on a study by Lemar et al.[1] The

inaccuracy of the above assumption is due to the glue being elastic-plastic in the measurement range of interest. Future calibration experiments should be performed in a matrix which is either completely plastic or hydrostatic. A suggested experiment is described below.

Future calibration experiments should be in the grooved configuration. This experiment is expected to generate more accurate inclusion analysis constants; fused silica remains elastic over the measurement range of the gauge. Inclusion analysis constants could then be determined from an elastic matrix assumption.

A recent observation has been the anistropy of ytterbium. This anisotropy is not accounted for in the piezoresistive model. In the future, to make experiments consistent and more accurate, the long part of pull test samples and the active area of gauges should be cut in same direction.

The use of ytterbium gauges was found to be time consuming. It takes a long time to perform the pull tests, calibration experiments, inclusion analysis, and explosive experiments. Other experimental techniques for measuring stress below 20 kbar insitu in explosives need to be explored.

CHAPTER 6

SUGGESTIONS FOR FUTURE WORK

Multiple ytterbium gauge experiments should be performed on PBXN-110 and PBXW-114 for stresses below 20 kbar. Stresses will be measured directly from the ytterbium gauges and calculated from the average shock speed. The unreacted Hugoniot of these explosives will be measured and compared to a preliminary Hugoniot obtained using quartz gauges.

The stress at which a low level reaction occurs will be determined. For stresses above this threshold, a reactive rate model will have to be used to predict explosive behavior. Thicker explosive plates should be used with diameters of about 3 inches. Stress-time profiles can be obtained deeper in the sample and shock velocities will be more accurate. A low level reaction may have a long run distance and be first seen at positions deeper in the explosive.

Future calibration experiments should be performed using fused silica compression-release experiments. Fused silica will allow the ytterbium gauges to calibrated to 20 kbar. Fused silica remains elastic to 20 kbar. It is recommended that gauges be placed in grooves machined into the fused silica. An elastic inclusion analysis can be performed to obtain certain required piezoresistive constants.

Reactive flow or SDT experiments should be performed to characterize the response of PBXN-110 and PBXW-114 for input stresses above 20 kbar. It is recommended that commercially available manganin gauges following the design of Lawerence Livermore National Laboratories[38] be used to make the required stress-time measurements. To insure a uniform (over time) response, it is recommended that gauges be constructed of manganin foil owned by NSWC. Calibration experiments to 200 kbars need to be performed to calibrate the gauges. An inclusion analysis should be used to obtain stress-time profiles from gauge records.

Future work must include testing of various explosive response models with the above proposed experimental work. Models should explain both the growth to full reaction (SDT) and low level burning. When appropriate model(s) are found, they should be implemented into hydrocodes. Calculated profiles should then be compared to experimental profiles.

A high frequency bridge circuit (see Appendix B) needs to be designed. This circuit will allow high resolution records to be obtained using Nicolet digitizers. The time required to obtain stress-time records is much shorter with Nicolet digitizers than with Tektronics oscilloscopes. This bridge circuit would be very helpful in recording signals in manganin gauge experiments. The voltage change due to gauge pressurization is a small fraction of the voltage drop caused by initial gauge resistance.

An improved inclusion analysis should be implemented. This analysis would treat an elastic-plastic matrix and would handle any arbitrary loading and unloading situation. The limitation of the present inclusion analysis is discussed in Appendix A.

Electromagnetic velocity gauge (EMV) measurements should be conducted at NSWC. Vorthman et al[8] at Los Alamos National Laboratory reported successful results in obtaining particle-velocity records in explosives using a gauge package they have developed. It is recommended that NSWC obtain Vorthman designed gauges to compare the results of particle velocity-time measurements with those of stress-time measurements in non-aluminized explosives.

The use of PVDF gauges[39] or manganin gauges to measure low level stress should be explored. The use of manganin gauges will require a high frequency bridge circuit and modifications to power supply[40] to provide for a constant current. Use of either of the above methods could mean that experiments would become much easier to construct and analyze.

Four channel, high resolution (5 nsec/pt) digitizers should be used to obtain gauge data. The faster digitizing rate and the increased voltage resolution of the high frequency bridge circuit described above would yield highly resolved voltage-time records. These records would end the need to digitize photographs of oscilloscope traces and, thus, shorten data analysis time. Future proposed Lagrange analysis requires a minimum of three (3) time correlated gauge records to be obtained simultaneously. These experiments would require significantly fewer digitizers if four channel digitizers were used.

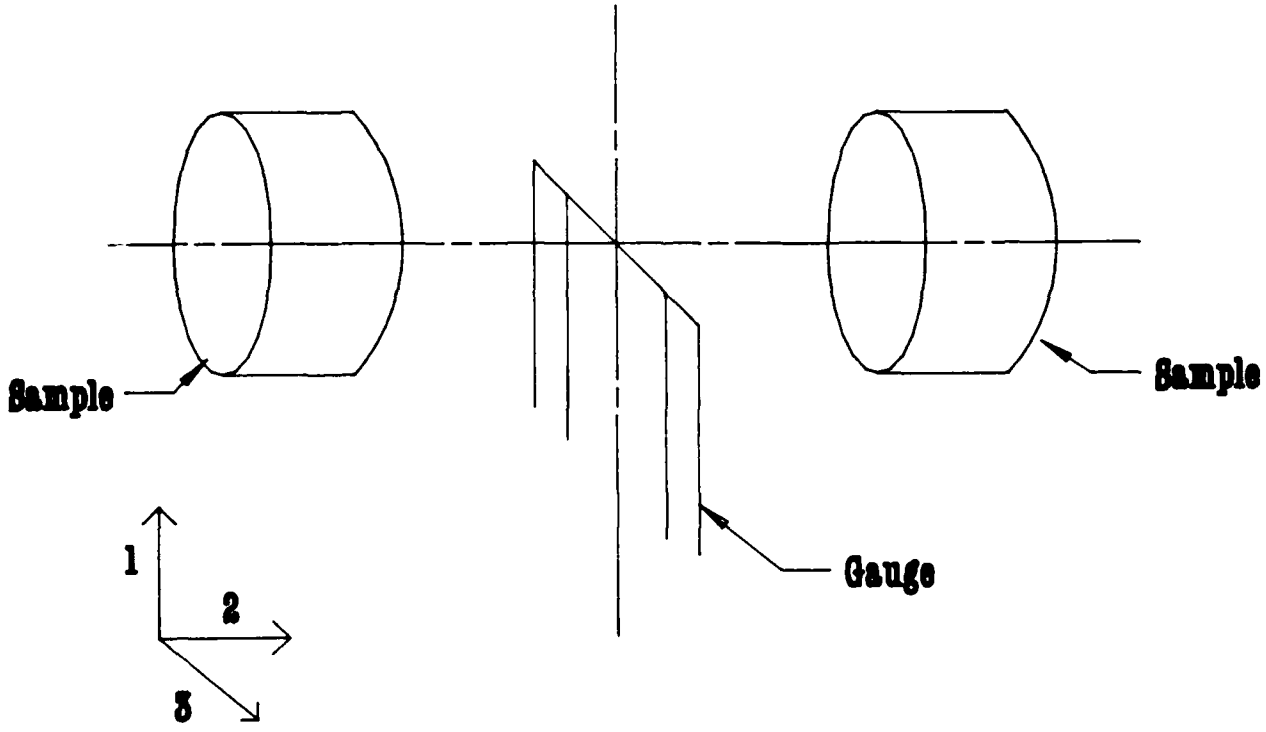

NOTE: DIRECTIONS ARE (1) ALONG WIDTH OF GAUGE, (2) ALONG THICKNESS OF GAUGE, AND (3) ALONG LENGTH OF GAUGE

FIGURE 1. EXPLODED VIEW OF AN INSITU GAUGE

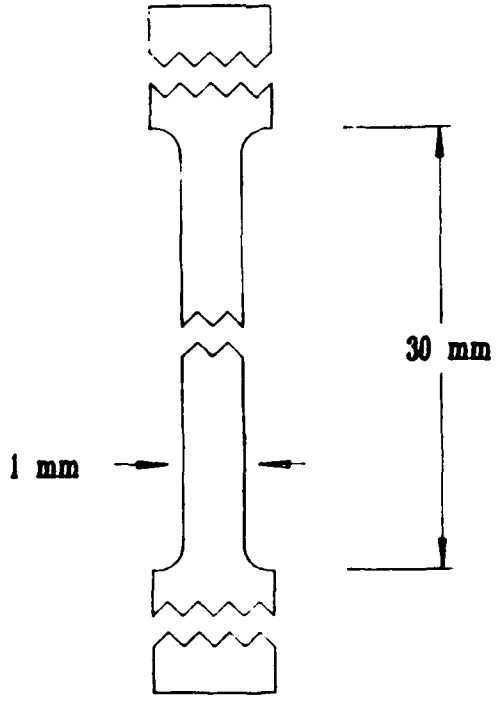

FIGURE 2. DRAWING SHOWING THE CONFIGURATION OF THE YTTERBIUM TEST SAMPLES THAT WERE "PULLED" IN QUASI-STATIC TESTING

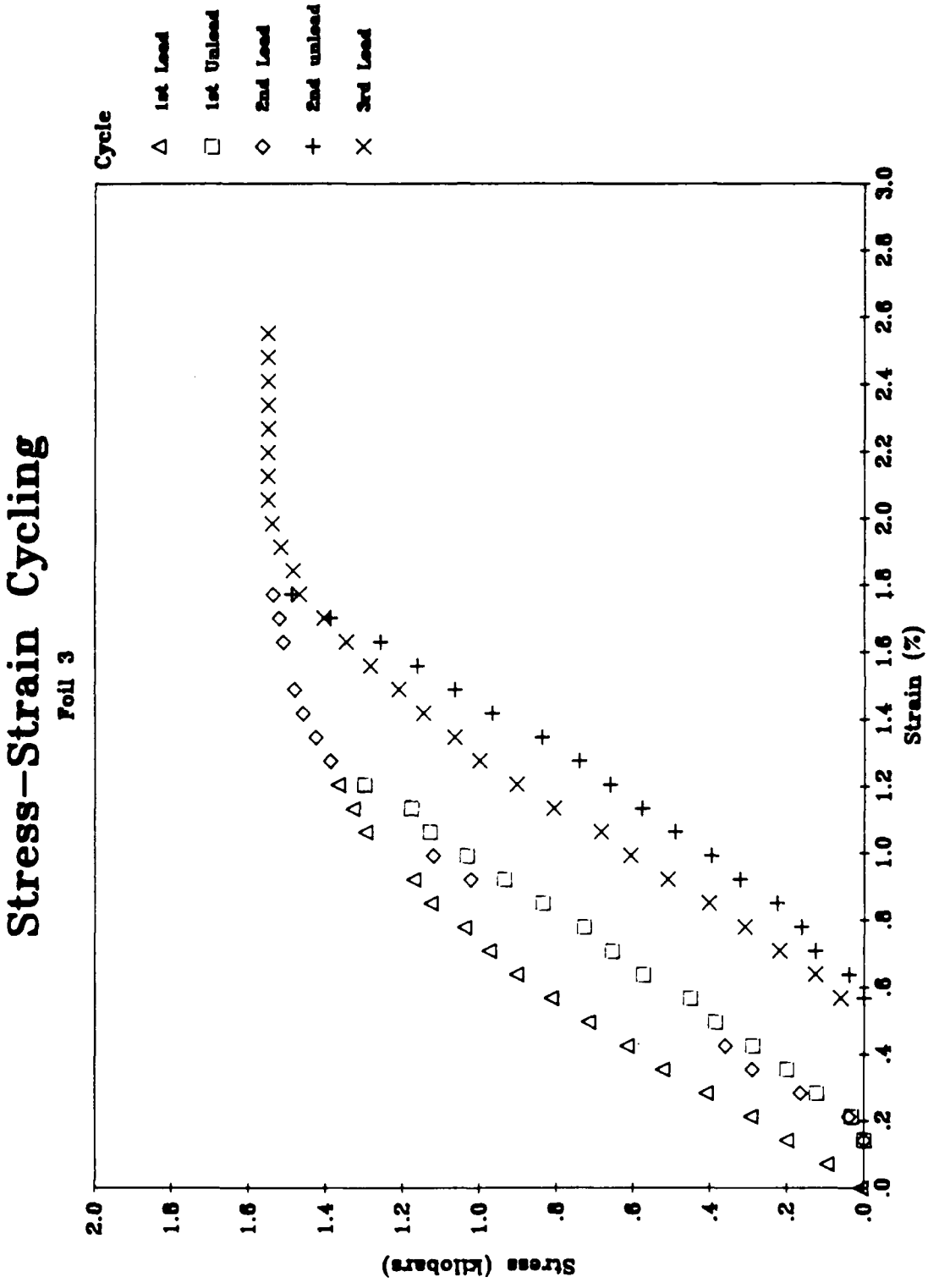

FIGURE 3. STRESS-STRAIN PLOT GENERATED DURING QUASI-STATIC TESTING

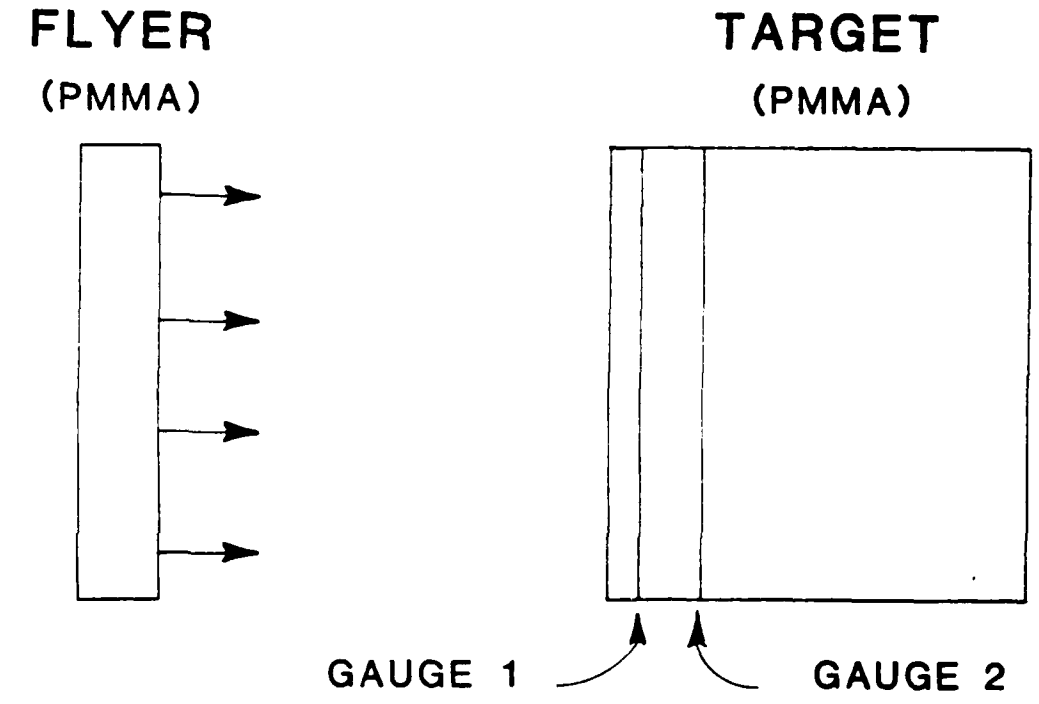

FIGURE 4. SCHEMATIC VIEW OF A PMMA SYMMETRIC IMPACT COMPRESSION-RELEASE EXPERIMENT

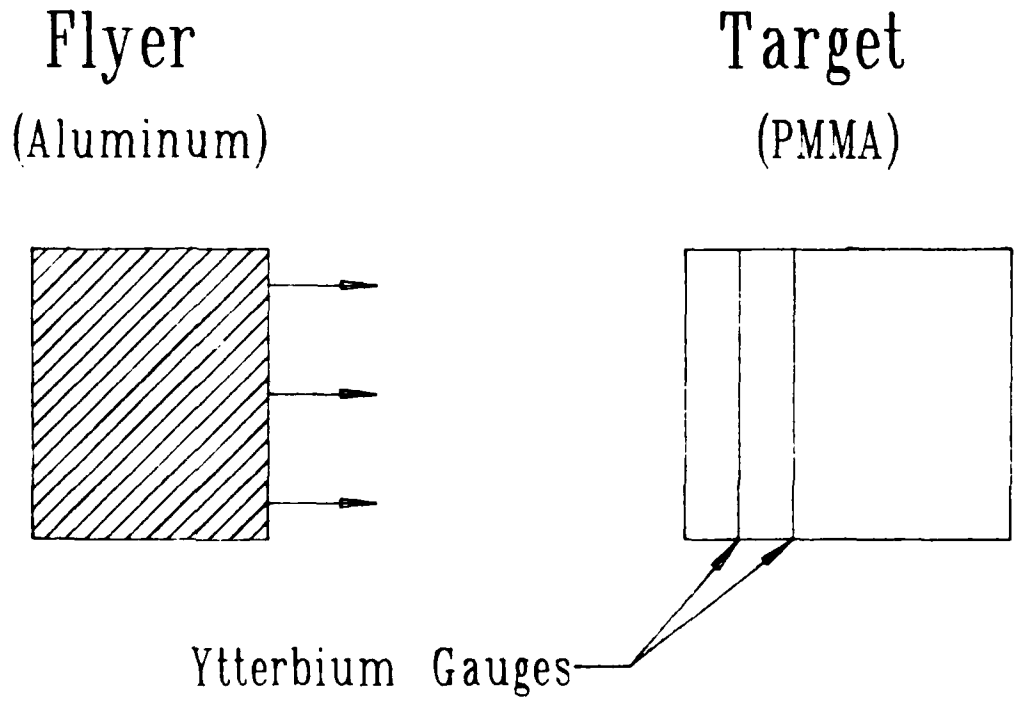

FIGURE 5. SCHEMATIC VIEW OF AN EXPERIMENT IN WHICH A THICK ALUMINUM FLYER IMPACTS A PMMA TARGET

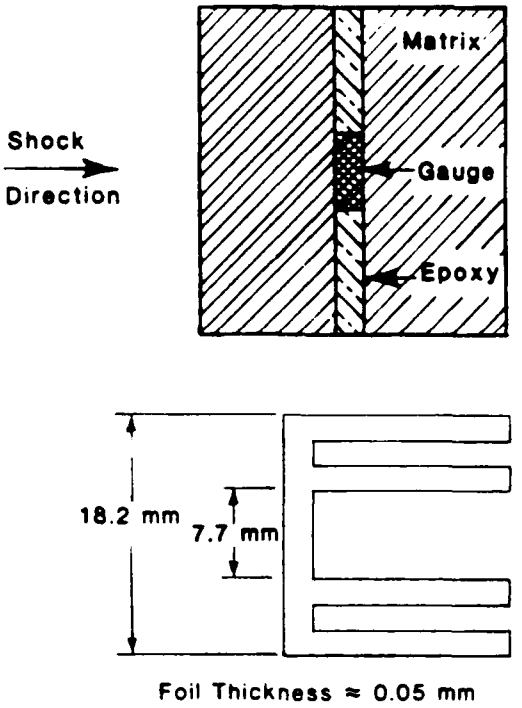

FIGURE 6. DIMENSIONS OF YTTERBIUM GAUGE AND SCHEMATIC REPRESENTATION OF THE YTTERBIUM GAUGE LOCATION WITHIN THE TARGET MATRIX

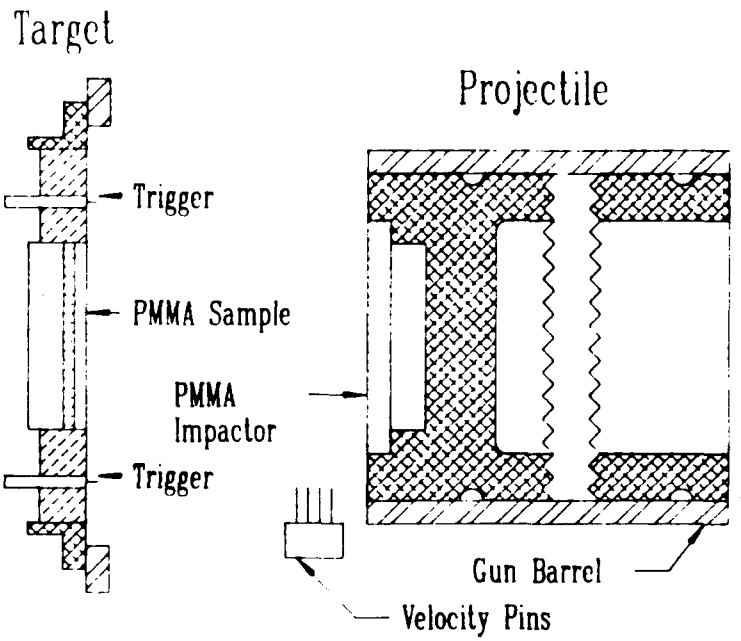

FIGURE 7. CUTAWAY VIEW OF TARGET AND PROJECTILE FOR A TYPICAL PMMA YTTERBIUM GAUGE CALIBRATION EXPERIMENT

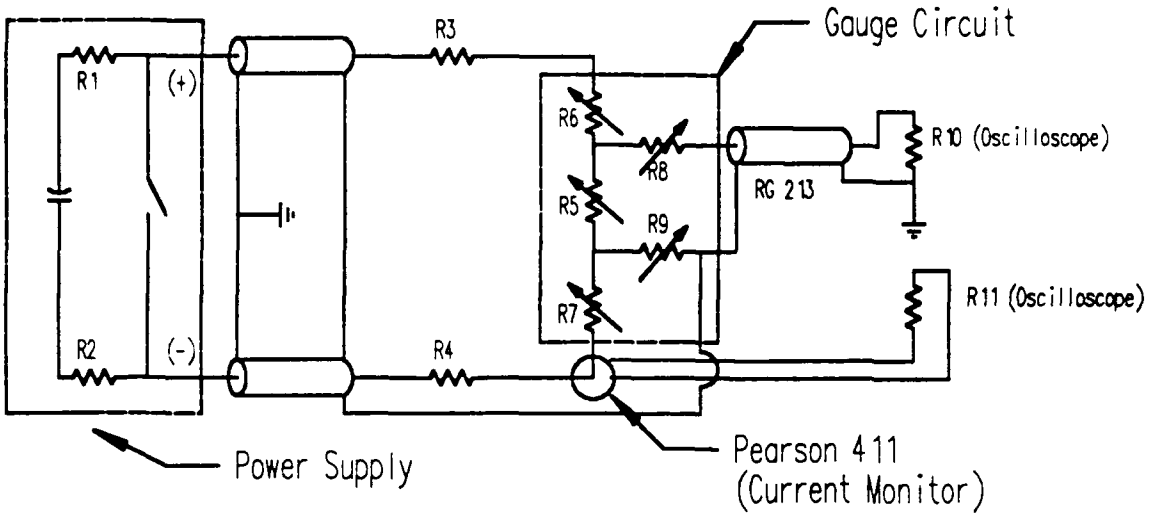

FIGURE 8. ELECTRICAL SCHEMATIC OF GAUGE POWER SUPPLY, EXPERIMENT, AND OSCILLOSCOPE

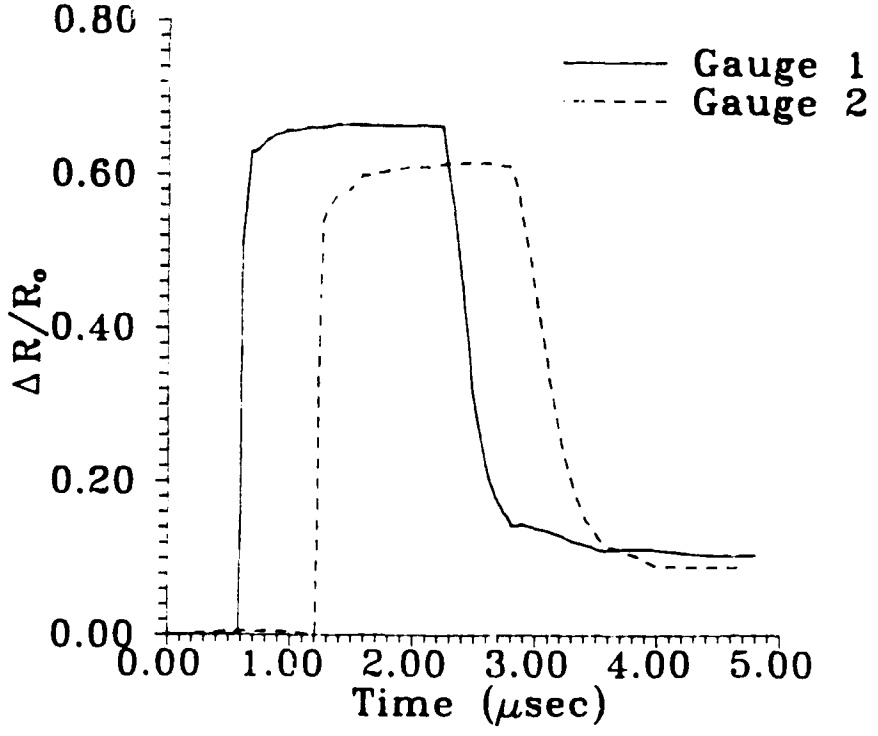

FIGURE 9. RELATIVE RESISTANCE CHANGE-TIME PROFILES FOR CALIBRATION EXPERIMENT 86-010

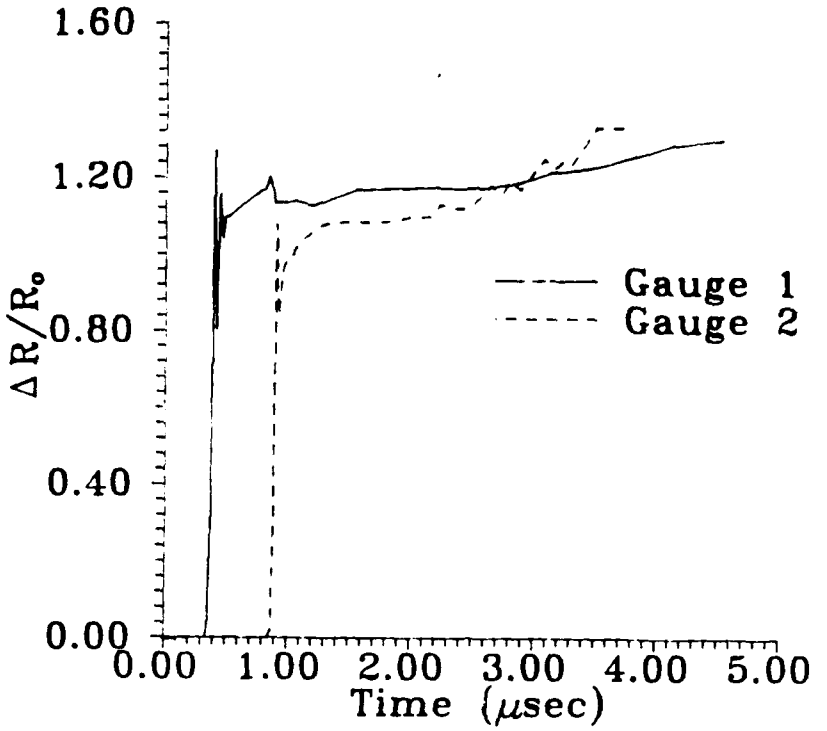

FIGURE 10. RELATIVE RESISTANCE CHANGE-TIME PROFILES FOR CALIBRATION EXPERIMENT 87-001

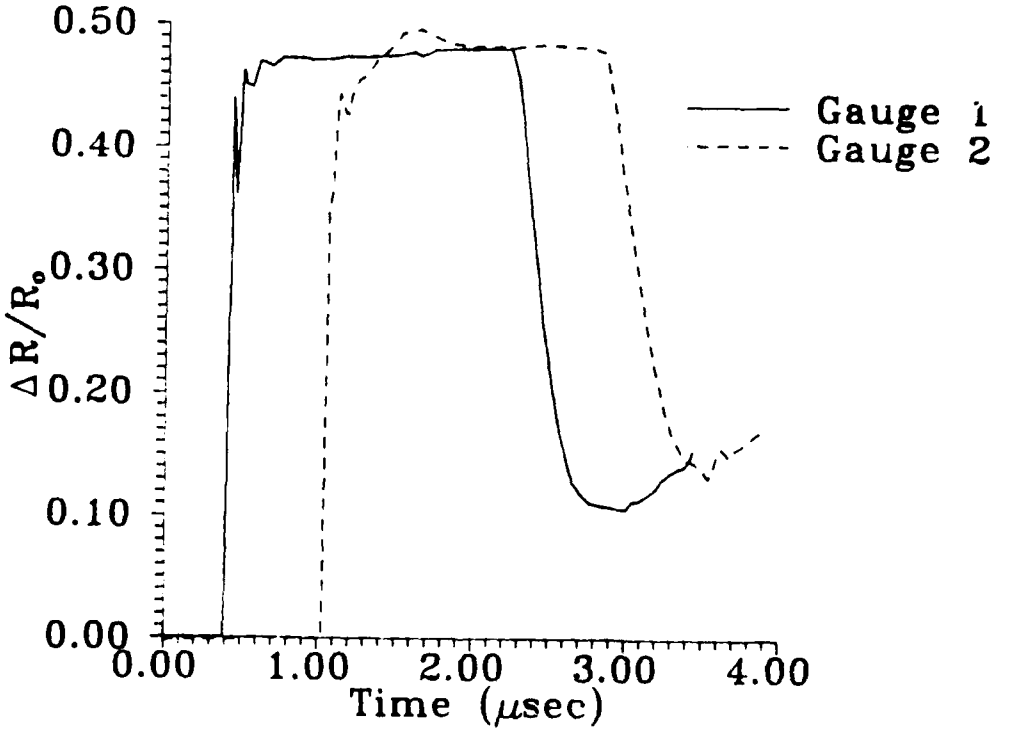

FIGURE 11. RELATIVE RESISTANCE CHANGE-TIME PROFILES FOR CALIBRATION EXPERMENT 87-002

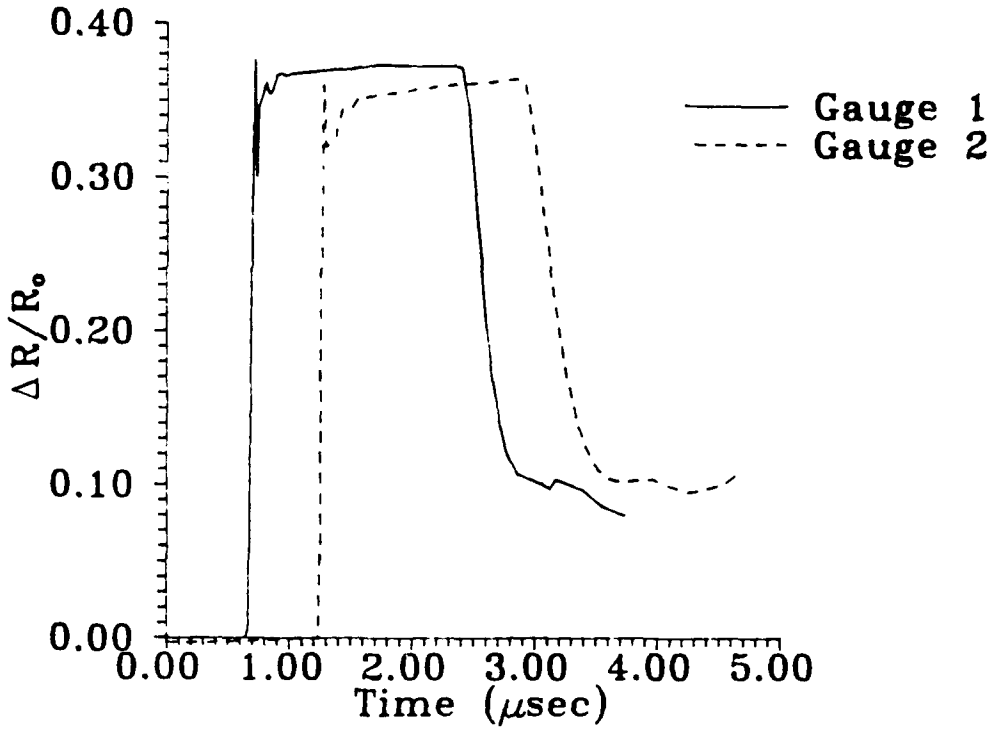

FIGURE 12. RELATIVE RESISTANCE CHANGE-TIME PROFILES FOR CALIBRATION EXPERIMENT 87-003

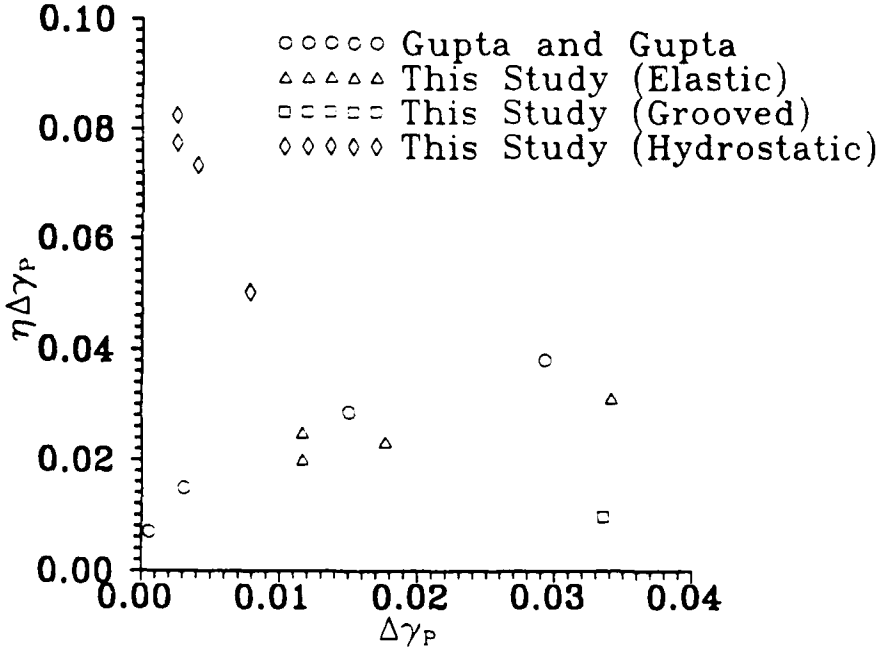

FIGURE 13. PLOT OF THE PRODUCT OF CONSTANT (η) AND THE ACCUMULATED PLASTIC STRAIN (γ_p) VS. THE ACCUMULATED PLASTIC STRAIN (γ)

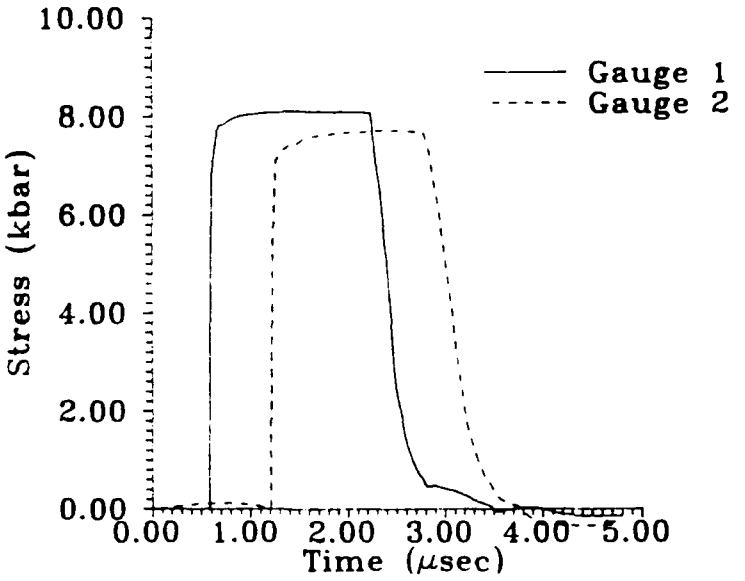

NOTE: INCLUSION ANALYSIS USED AN ELASTIC MATRIX ASSUMPTION.

FIGURE 14. STRESS-TIME RECORD OBTAINED FROM USING AN INCLUSION ANALYSIS TO ANALYZE THE $\Delta R/R_0$ RECORD OBTAINED FROM EXPERIMENT 86-010

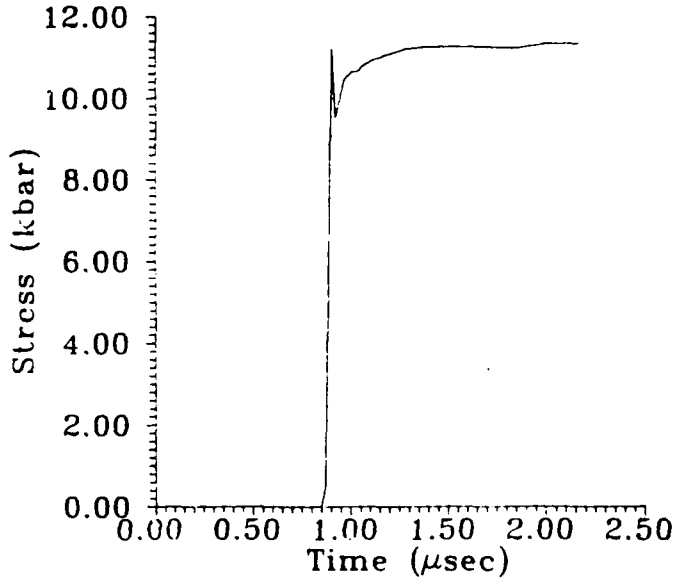

NOTE: INCLUSION ANALYSIS USED AN ELASTIC MATRIX ASSUMPTION.

FIGURE 15. STRESS-TIME RECORD OBTAINED FROM USING AN INCLUSION ANALYSIS TO ANALYZE THE $\Delta R/R_0$ RECORD OBTAINED FROM EXPERIMENT 87-001

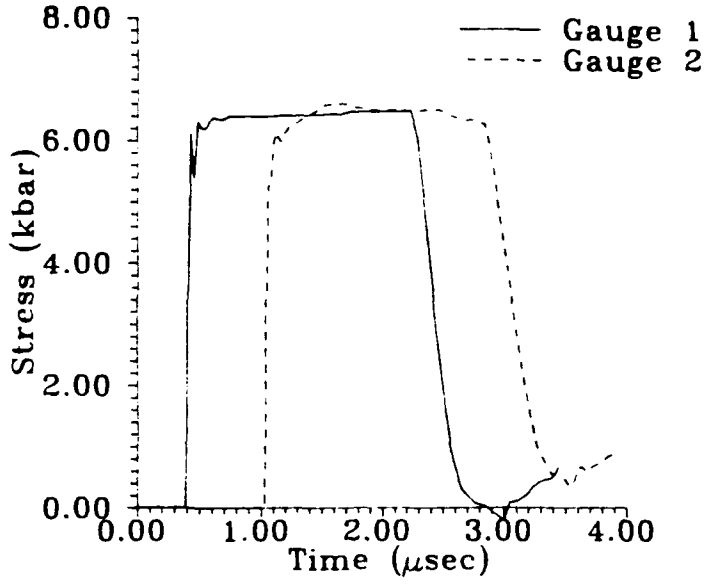

NOTE: INCLUSION ANALYSIS USED AN ELASTIC MATRIX ASSUMPTION.

FIGURE 16. STRESS-TIME RECORD OBTAINED FROM USING AN INCLUSION ANALYSIS TO ANALYZE THE $\Delta R/R_0$ RECORD OBTAINED FROM EXPERIMENT 86-002

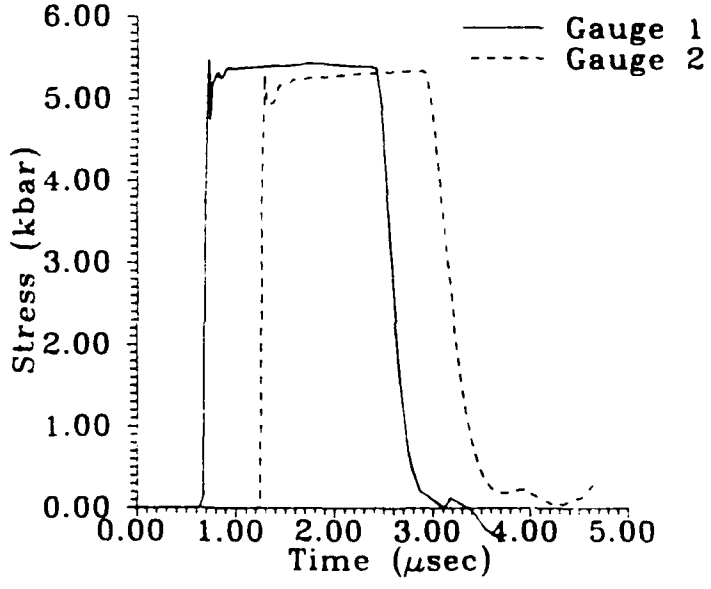

NOTE: INCLUSION ANALYSIS USED AN ELASTIC MATRIX ASSUMPTION.

FIGURE 17. STRESS-TIME RECORD OBTAINED FROM USING AN INCLUSION ANALYSIS TO ANALYZE THE $\Delta R/R_0$ RECORD OBTAINED FROM EXPERIMENT 86-003

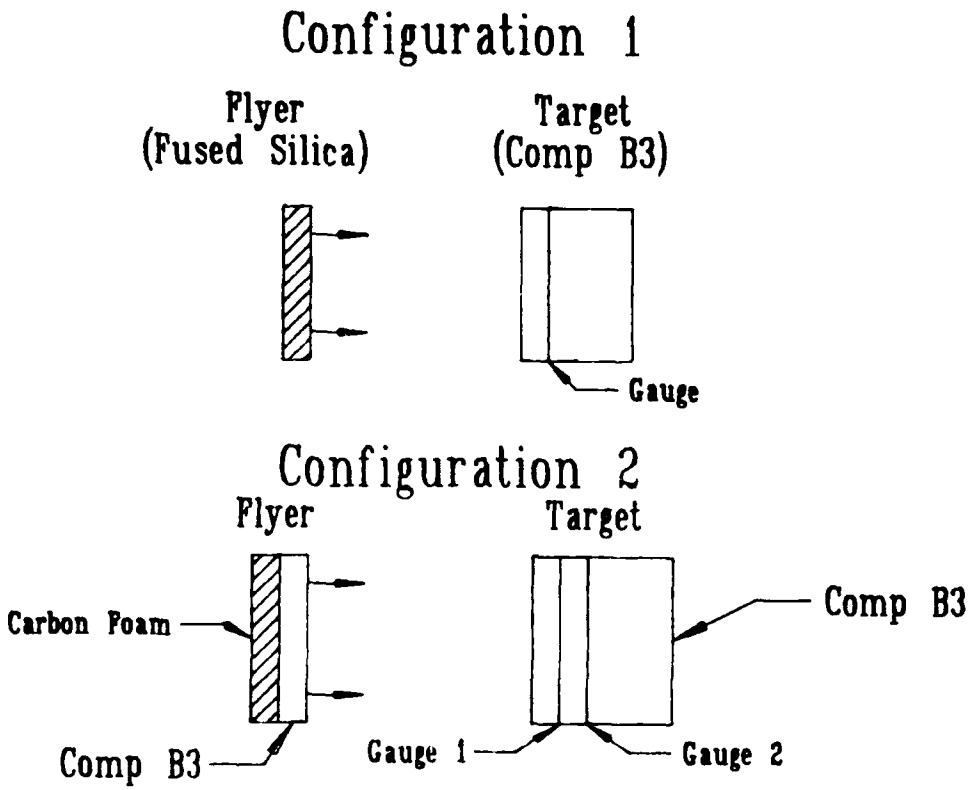

FIGURE 18. SCHEMATIC DRAWING OF THE TWO EXPERIMENTAL CONFIGURATIONS USED IN EXPLOSIVE EXPERIMENTS

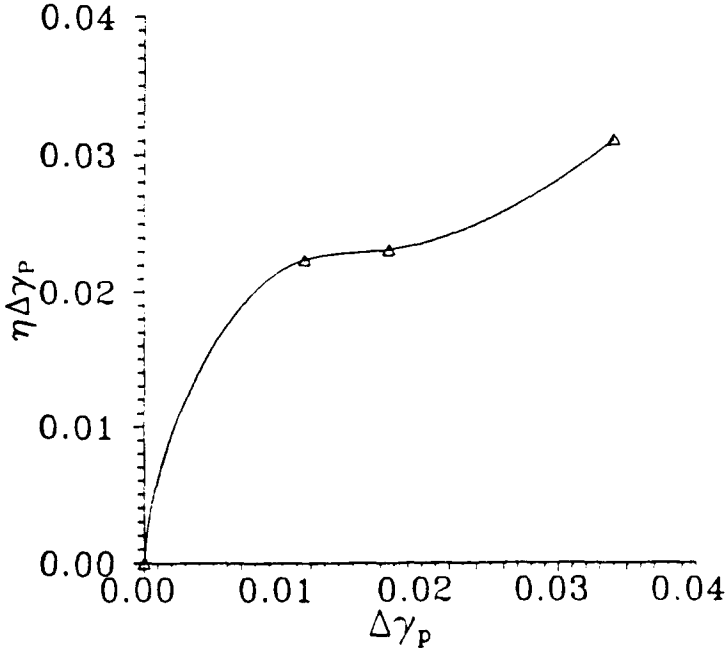

FIGURE 19. PLOT OF THE PRODUCT OF CONSTANT (η) AND THE ACCUMULATED PLASTIC STRAIN (γ_p) VS. THE ACCUMULATED PLASTIC STRAIN (γ_p) FROM EXPERIMENTS OF THIS STUDY

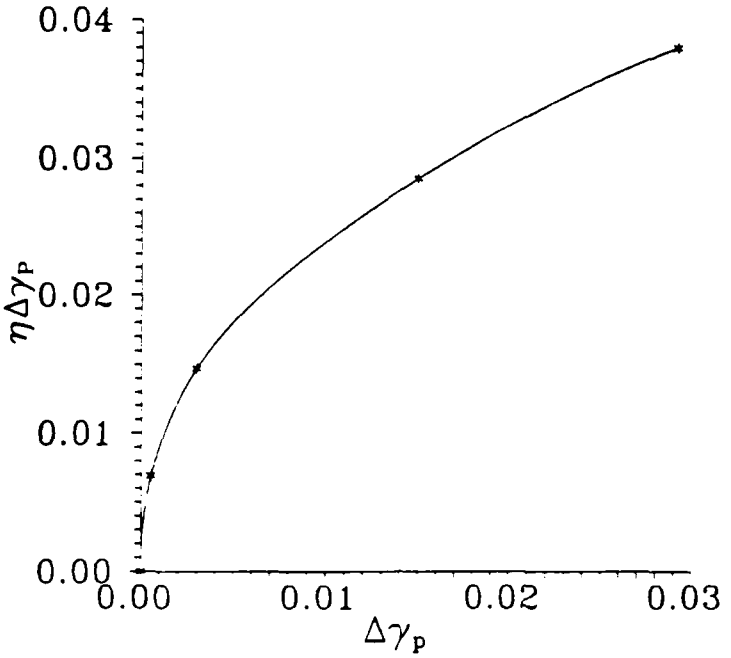

FIGURE 20. PLOT OF THE PRODUCT OF CONSTANT(η) AND THE ACCUMULATED PLASTIC STRAIN (γ_p) VS. THE ACCUMULATED PLASTIC STRAIN (γ_p) FROM EXPERIMENTS OF GUPTA AND GUPTA (REF.28)

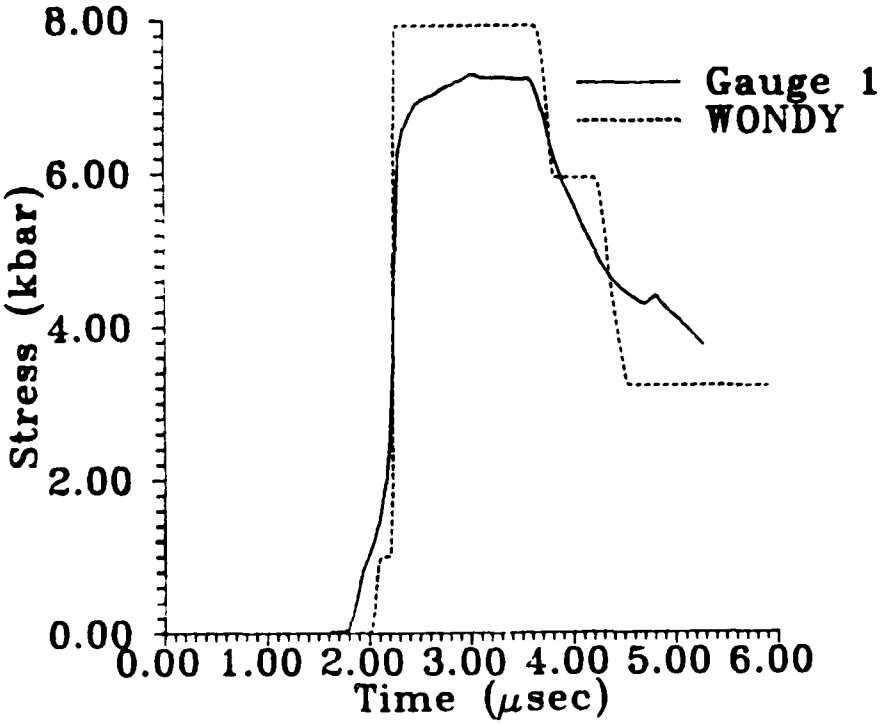

NOTE: INCLUSION ANALYSIS USED PARAMETERS m AND η FROM THIS STUDY.

FIGURE 21. EXPERIMENTAL AND CALCULATED STRESS-TIME PROFILES FOR EXPERIMENT 87-004

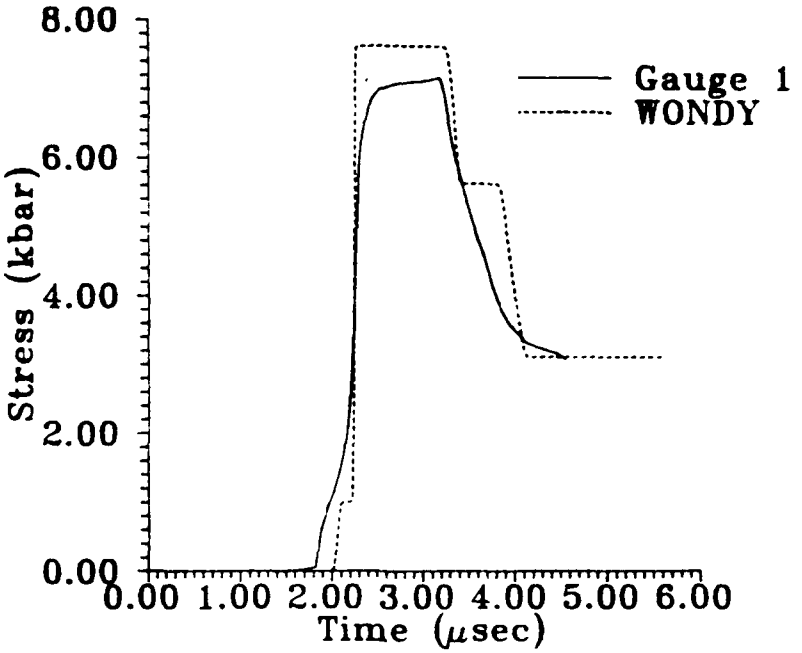

NOTE: INCLUSION ANALYSIS USED PARAMETERS m AND η FROM THIS STUDY.

FIGURE 22. EXPERIMENTAL AND CALCULATED STRESS-TIME PROFILES FOR EXPERIMENT 87-008

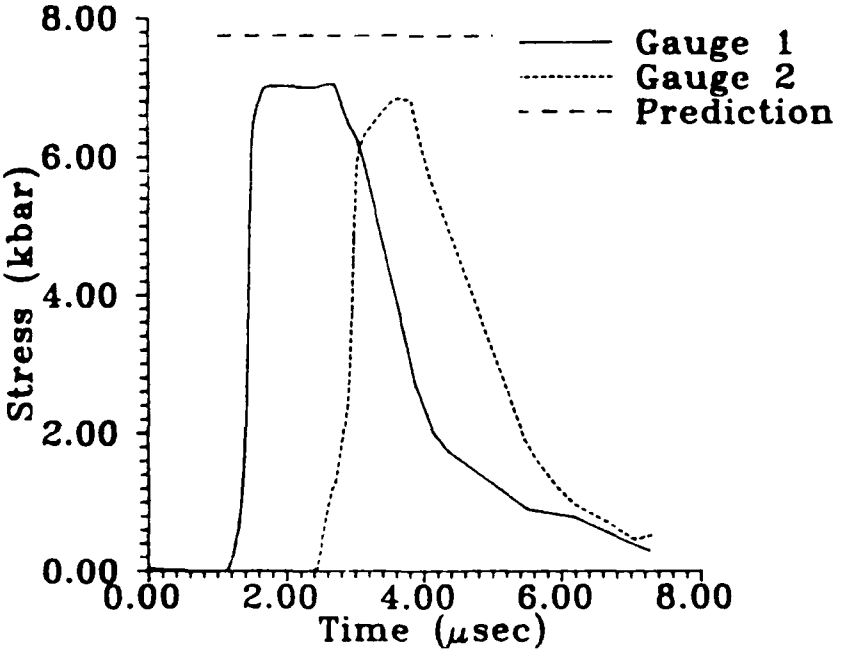

NOTE: INCLUSION ANALYSIS USED PARAMETERS m AND η FROM THIS STUDY
PREDICTION IS BASED ON THE CALCULATION FROM LEMAR et al's HUGONIOT (REF. 1)

FIGURE 23. EXPERIMENTAL STRESS-TIME PROFILES FOR EXPERIMENT 87-009

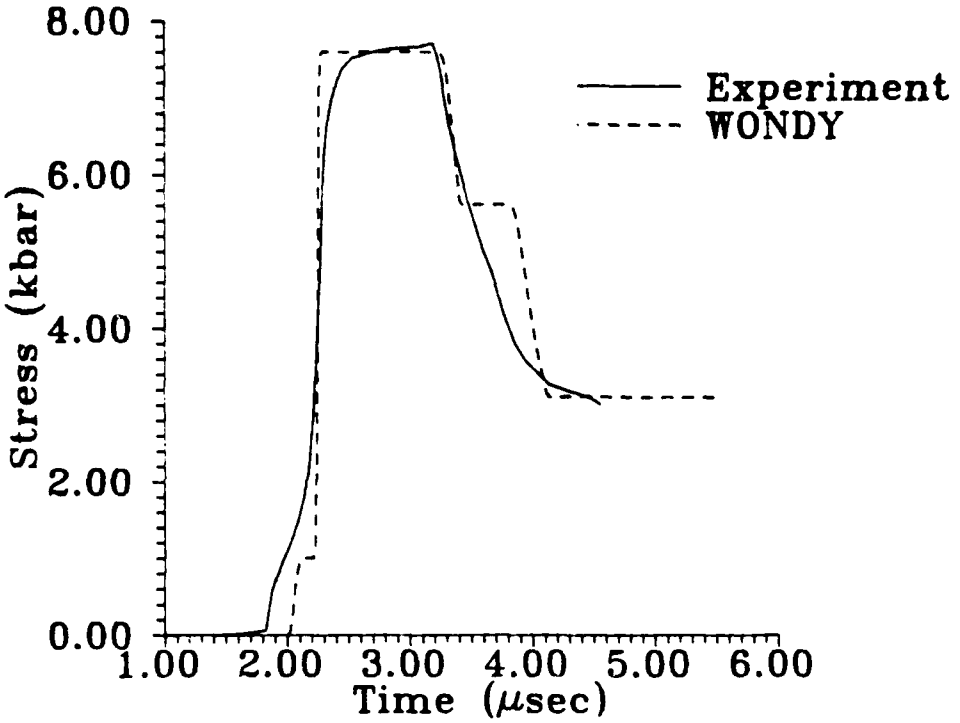

NOTE: INCLUSION ANALYSIS USED PARAMETERS m AND η FROM GUPTA AND GUPTA (REF. 28).

FIGURE 24. EXPERIMENTAL AND CALCULATED STRESS-TIME PROFILES FOR EXPERIMENT 87-004

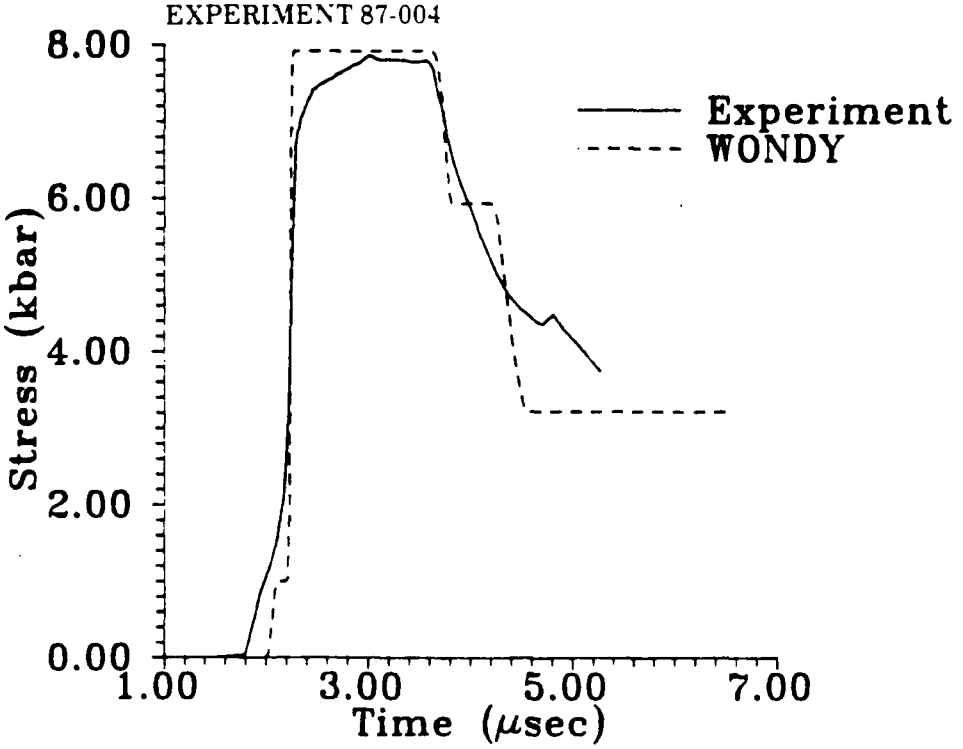

NOTE: INCLUSION ANALYSIS USED PARAMETERS m AND η FROM GUPTA AND GUPTA (REF. 28)

FIGURE 25. EXPERIMENTAL AND CALCULATED STRESS-TIME PROFILES FOR EXPERIMENT 87-008

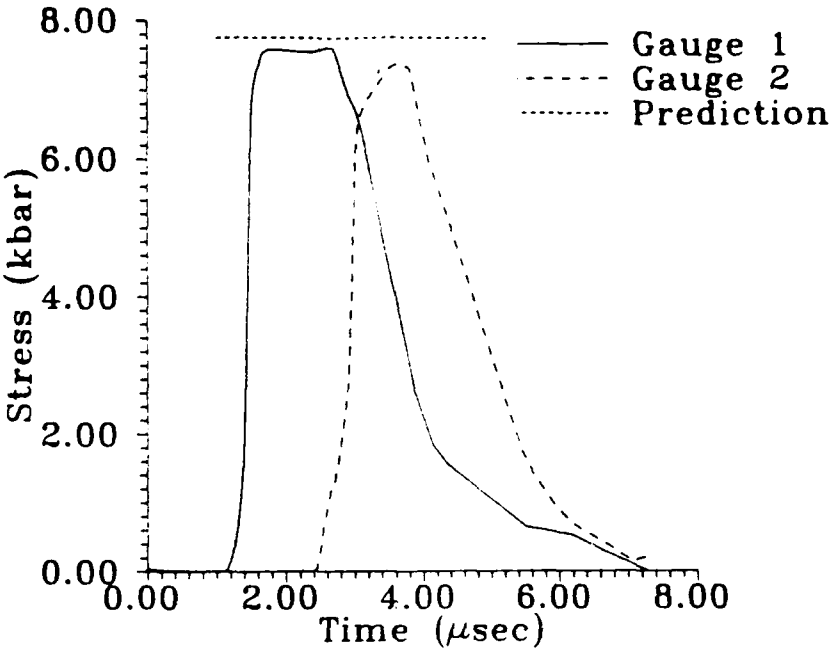

NOTE: INCLUSION ANALYSIS USED PARAMETERS m AND η FROM GUPTA AND GUPTA (REF. 28). PREDICTION IS BASED ON CALCULATION FROM LEMAR et al's HUGONIOT (REF. 1).

FIGURE 26. EXPERIMENTAL STRESS-TIME PROFILES FOR EXPERIMENT 87-009

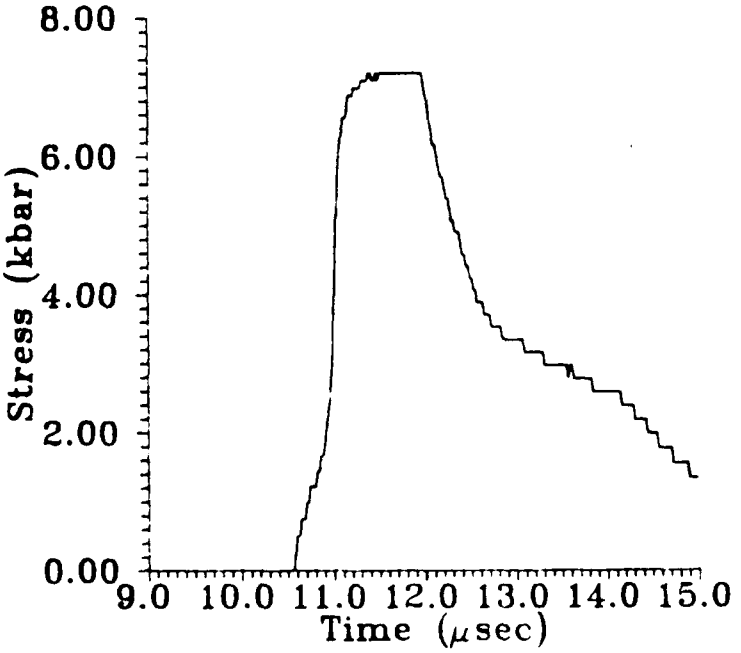

NOTE: INCLUSION ANALYSIS USED PARAMETERS m AND η FROM THIS STUDY.

FIGURE 27. EXPERIMENTAL STRESS-TIME PROFILE OBTAINED WITH THE USE OF A NICOLET DIGITIZER FOR EXPERIMENT 87-008

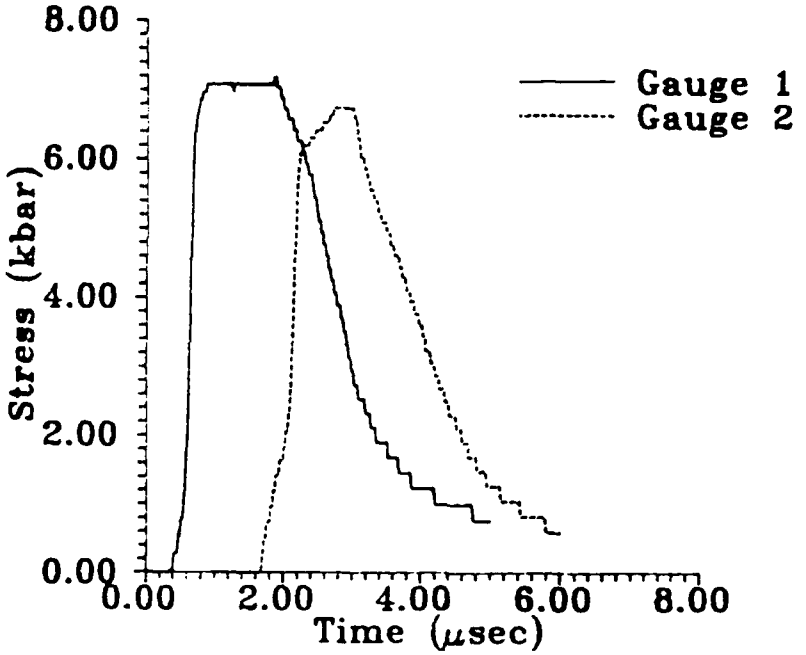

NOTE: INCLUSION ANALYSIS USED PARAMETERS m AND η FROM THIS STUDY.

FIGURE 28. EXPERIMENTAL STRESS-TIME PROFILES OBTAINED WITH THE USE OF A NICOLET DIGITIZER FOR EXPERIMENT 87-009

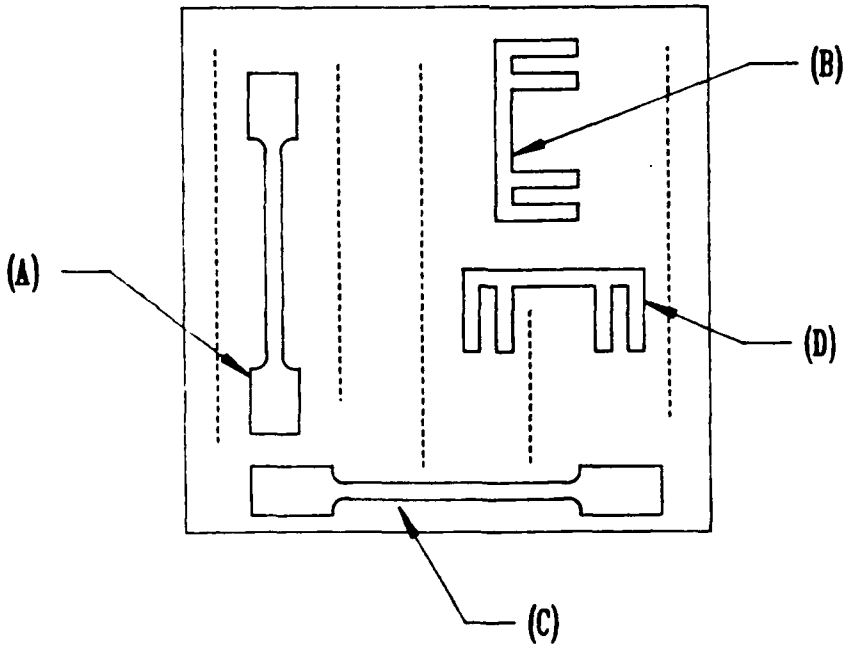

FIGURE 29. TWO ORIENTATIONS IN WHICH TENSILE TEST SAMPLES AND GAUGES CAN BE CUT OUT OF THE YTTERBIUM FOILS

TABLE 1. EXPLOSIVE FORMULATIONS

Explosive	Ingredients	Wt.%
Composition B-3[1]	RDX	60
	TNT	40
PBX-9404[41]	HMX	94
	Nitrocellulose	3
	CEF Plasticizer	3
PBXN-110 (PBXW-113)[42]	HMX	88
	Polyurethane Binder	12
PBXW-109[42]	RDX	65
	Aluminum	20
	Plasticizer (diadipate)	7
	Polyurethane Binder	7
PBXW-114[42]	HMX	78
	Aluminum Powder	10
	Polyurethane Binder	12

TABLE 2. MEASURED FOIL THICKNESS

Foil #	Thickness (10^{-3} cm)
1	4.70
2	4.73
3	4.74
4	4.78
5	5.41*
6	4.69
7	4.80
8	4.83
9	4.68
10	4.63
Mean	4.73 ± 0.06

* The larger thickness of foil 5 is probably because the manufacturer used a different roller gap than used for the other foils.

TABLE 3. MEASURED FOIL CONSTANTS

Foil	Yield Strength (kbar)	Young's Modulus (E) (kbar)	$\pi_{11}\|_o$ ($kbar^{-1}$)	$\pi_{12}\|_o$ ($kbar^{-1}$)	η
1	0.75	156.7	-0.04121	-0.008267	0.52
3	0.92	147.8	-0.04226	-0.007743	0.88
4	0.90	160.4	-0.03841	-0.009668	0.79
5	----	123.0	-0.03833	-0.009711	----
6	0.84	161.7	-0.03941	-0.009168	----
7	0.82	154.5	-0.04065	-0.008548	----
8	0.82	178.5	-0.04087	-0.008440	----

TABLE 4. MEAN MEASURED FOIL CONSTANTS

Yield Strength	0.84 ± 0.06 kbar
Young's Modulus (E)	154.7 ± 16.8 kbar
Bulk Modulus (K)	148.0 kbar
Shear Modulus (G)	58.3 kbar
$\pi_{11}\|_o$	-0.04016 ± 0.00138 $kbar^{-1}$
$\pi_{12}\|_o$	-0.008792 ± 0.000743 $kbar^{-1}$
η	0.73

TABLE 5. CALIBRATION EXPERIMENTAL PARAMETERS

Shot #	Projectile Velocity (mm μsec^{-1})	Particle Velocity (mm μsec^{-1})	Stress (kbar)	Strain
86-010	0.4402	0.2201	8.19	0.0702
87-001	0.3952	0.3181	11.91	0.1018
87-002	0.3406	0.1703	6.29	0.0547
87-003	0.3017	0.1508	5.51	0.0490

TABLE 6. MEASURED PEAK AND RESIDUAL RESISTANCE CHANGES

Experiment Number	Gauge Number	Peak $\Delta R/R_o$	Residual $\Delta R/R_o$
86-010	1	0.665	0.110
	2*	0.615	0.089
87-001	1**	1.077	-----
	2	1.176	-----
87-002	1	0.481	0.105
	2†	0.484	-----
87-003	1	0.374	0.102
	2	0.365	0.097

*Gauge was placed in a groove cut in the PMMA matrix.
**Gauge was not surrounded by matrix material.
†An increase in gauge current rendered residual $\Delta R/R_o$ measurement inaccurate.

TABLE 7. INCLUSION ANALYSIS PARAMETERS FOR AN ELASTIC MATRIX

Shot Number	Gauge Number	Shear Modulus μ (kbar)	Bulk Modulus K (kbar)	m ($kbar^{-2}$) (10^{-3})	η
86-010	1	25.93	82.10	1.18	0.91
	2 (in groove)	23.70	85.60	0.97	0.28
87-002	1	25.93	80.42	1.50	1.31
	2	25.93	80.42	*	*
87-003	1	25.93	77.88	1.01	1.72
	2	25.93	77.88	1.07	2.14

*The constants m and η could not be measured because of a late time increase in gauge current.

TABLE 8. INCLUSION ANALYSIS PARAMETERS FOR A HYDROSTATIC MATRIX

Shot Number	Gauge Number	Shear Modulus μ (kbar)	Bulk Modulus K (kbar)	m ($kbar^{-2}$) (10^{-3})	η
86-010	1	0.0001*	116.7	0.847	6.45
87-002	1	0.0001*	115.0	0.700	18.5
	2	0.0001*	115.0	**	**
87-003	1	0.0001*	112.5	0.030	33.2
	2	0.0001*	112.5	†	31.2

*A shear modulus of zero gives large computational errors in the inclusion analysis code. Therefore, a small shear modulus is used.
**The constants m and η could not be measured because of a late time increase in gauge current.
†A negative value of the constant m would be needed to yield the correct initial relative resistance change.

TABLE 9. PEAK STRESSES CALCULATED FROM INCLUSION ANALYSIS (ELASTIC MATRIX ASSUMPTION)

Shot Number	Stress Gauge 1 (kbar)	Error Gauge 1 (%)	Stress Gauge 2 (kbar)	Error Gauge 2 (%)
86-010	8.11	- 0.9	7.73	- 5.6
87-011	----	---	11.25	- 5.0
87-002	6.48	3.0	6.61	5.1
87-003	5.44	- 1.2	5.34	- 3.1

TABLE 10. EXPERIMENTAL PARAMETERS FOR EXPLOSIVE EXPERIMENTS

Shot Number	Configuration	Projectile Velocity (mm/μsec)	Peak Expected Stress (kbar)
87 - 004	1	0.2339	7.92
87 - 008	1	0.2254	7.62
87 - 009	2	0.3367	7.75
87 - 010	2	0.3003	6.85

TABLE 11. EXPLOSIVE EXPERIMENT PLATE THICKNESS

	Projectile		Target		
Shot Number	Impactor Thickness (mm)	Impactor Type	Front Piece Thickness (mm)	Mid Piece Thickness (mm)	Back Piece Thickness (mm)
87-004	6.373	Fused Silica	5.975	-----	9.909
87-008	5.194	Fused Silica	5.967	-----	9.865
87-009	3.023	Comp B-3	2.027	3.998	9.883

TABLE 12. EXPLOSIVE INCLUSION ANALYSIS PARAMETERS

Experiment Number	Shear Modulus μ (kbar)	Bulk Modulus K (kbar)	γ_p	η^*	η^{28}
87-004	1.00	120.50	0.0081	2.47	2.85
87-008	1.00	119.43	0.0078	2.51	2.78
87-009	1.00	119.79	0.0076	2.52	2.69

All explosive experiments

m (This study)	0.00124 $kbar^{-1}$
m (Gupta et al[28])	0.00076 $kbar^{-1}$
$\pi_{11}\|_o$	-0.04016 $kbar^{-1}$
$\pi_{12}\|_o$	-0.008792 $kbar^{-1}$
Ytterbium Yield Strength	0.84 kbar
Ytterbium Bulk Modulus	148.0 kbar
Ytterbium Shear Modulus	58.3 kbar

*From dynamic calibration experiments of this study.

TABLE 13. PREDICTED AND EXPECTED EXPLOSIVE STRESS USING η AND m FROM THIS STUDY

Experiment	Predicted Stress (kbar)	Measured Stress Gauge 1 (kbar)	Measured Stress Gauge 2 (kbar)	Stress from Shock Vel. Gauge 1 (kbar)	Stress from Shock Vel. Gauge 2 (kbar)
87-004	7.92	7.2	---	-----	-----
87-008	7.62	7.1	---	-----	-----
87-009	7.75	7.0	6.8	7.84	7.84

Percent Deviation From Predicted Stress

Experiment	Measured Stress Deviation Gauge 1 (%)	Measured Stress Deviation Gauge 2 (%)	Stress from Shock Vel. Deviation Gauge 1 (%)	Stress from Shock Vel. Deviation Gauge 2 (%)
87-004	-9.1	-----	-----	-----
87-008	-6.8	-----	-----	-----
87-009	-9.7	-12.3	+1.2	+1.2

TABLE 14. PREDICTED AND EXPECTED EXPLOSIVE STRESS USING η AND m FROM REF. 28

Experiment	Predicted Stress (kbar)	Measured Stress Gauge 1 (kbar)	Measured Stress Gauge 2 (kbar)	Stress from Shock Vel. Gauge 1 (kbar)	Stress from Shock Vel. Gauge 2 (kbar)
87-004	7.92	7.8	---	-----	-----
87-008	7.62	7.6	---	-----	-----
87-009	7.75	7.5	7.3	7.84	7.84

Percent Deviation From Predicted Stress

Experiment	Measured Stress Deviation Gauge 1 (%)	Measured Stress Deviation Gauge 2 (%)	Stress from Shock Vel. Deviation Gauge 1 (%)	Stress from Shock Vel. Deviation Gauge 2 (%)
87-004	-1.5	-----	-----	-----
87-008	-0.3	-----	-----	-----
87-009	-3.2	-5.8	+1.2	+1.2

TABLE 15. MEASURED WAVE VELOCITIES FOR EXPERIMENT 87-009

Elastic Shock Velocity -	3.14 mm/μsec
Plastic Shock Velocity (Lagrangian) -	2.65 mm/μsec
Sound Speed upon Release (Lagrangian) -	3.54 mm/μsec
Sound Speed upon Release (Eulerian) -	3.30 mm/μsec

REFERENCES

1. Lemar, E. R., et al, "Unreacted Hugoniot of Composition B-3 for Stresses of 0-16 kbar," Journal of Applied Physics, Vol. 58, No. 9, 1985, pp. 3404-3408.

2. Lemar, E. R.; Forbes, J. W.; and Sutherland, G.T., "Unreacted Hugoniot of PBXW-113 (Type II) and PBXW-114 (Type II) Explosive for Stresses of 0-16 kbar," Bull. APS, Vol. 31, Apr 1985, p. 824.

3. Nunziato, J. W.; Kennedy, J. E.; and Hardesty, D. R., "Modes of Shock Wave Growth in the Initiation of Explosives," in Proceedings of the Sixth Symposium on Detonation, 24-27 Aug 1976, pp. 47-59.

4. Wackerle, J., et al, "A Shock Initiation Study of PBX 9404," in Proceedings of the International Symposium on High Dynamic Pressures, Paris, France, 27-31 Aug 1978, pp. 127-138.

5. Olinger, B., and Hopson, J. W., in Proceedings of the International Symposium on High Dynamic Pressures, Paris, France, 1979, pp. 9-19.

6. Weingart, R. C., "Basic Research on High-Explosive Initiation," Energy and Technology Review, Lawrence Livermore National Laboratory publication UCRL-52000-78-9, Sep 1987, pp. 1-6.

7. Cowperthwaite, M., and Gupta, Y. M., "Investigation of Shear Induced Reaction in Composition B-3," Shockwaves in Condensed Matter, edited by Gupta, Y. M., Plenum Press, New York, NY, 1986.

8. Vorthman, J.; Andrews, G.; and Wackerle, J., "Reaction Rates from Electromagnetic Gauge Data" in Proceedings of the Eighth Symposium on Detonation, 15-19 Jul 1985, pp. 99-110.

9. Bridgeman, P. W., Proc. of the Amer. Acad. Arts Sci., Vol. 47, 1911, pp. 321-342.

10. Bridgeman, P. W., The Physics of High Pressure, London, G. Bell and Sons Ltd., 1958.

11. Fuller, P. J. A., and Price, J. H., Nature, Vol. 193, 1962, pp. 262-263.

12. Keough, D. D., SRI final report, DASA Contract no. 69-C-0014, 1970.

REFERENCES (Cont.)

13. Keough, D. D., Development of a High-Sensitivity Piezoresistive Stress Transducer of the Low Kilobar Range, Final Report, Contract DNA001-72-C-0146, Stanford Research Institute International, Menlo Park, CA, 1973.

14. Ginsberg, M. J., et al, Effects of Stress on the Electrical Resistance of Ytterbium and Calibration of Ytterbium Stress Transducers, Final Report, Contract DNA001-72-C-0146, Stanford Research Institute International, Menlo Park, CA, 1973.

15. Gupta, Y. M., "Stress measurements using piezoresistance gauges: Modeling the gauge as an elastic-plastic inclusion," Journal of Applied Physics, Vol. 54, No. 11, 1983, pp. 6256-6266.

16. Gupta, S. C., and Gupta, Y. M., "Piezoresistance response of longitudinally and laterally oriented ytterbium foils subjected to impact and quasi-static loading," Journal of Applied Physics, Vol. 57, No. 7, 1985, pp. 2464-2472.

17. Sutherland, G.T., private communication with Y. M. Gupta of Washington State University concerning the pressure dependence of the piezoresistive coefficients, Sep 1988.

18. Brar, N. S., and Gupta, Y. M., "Piezoresistance response of ytterbium foil gauges shocked to 45 kbar in fused silica matrix," Journal of Applied Physics, Vol. 61, No. 4, 1987.

19. Carter, W. J., et al, Journal of Physical Chemistry, Vol. 36, 1975, p. 741.

20. Pearson, C. E., Theoretical Elasticity, Harvard University Press, 1959.

21. Chen, D. Y.; Gupta, Y. M.; and Miles M. H., "Quasi-static experiments to determine material constants for the piezoresistance foils used in shock wave experiments," Journal of Applied Physics, Vol. 55, No. 11, 1984, pp. 3984-3993.

22. Sutherland, G. T., unpublished Computer Code DREDUCE, Naval Surface Warfare Center, 1987.

23. Tasker, D. G., unpublished Computer Code GNIC, Naval Surface Warfare Center, 1987.

24. Keough, D. D., "Procedure for Fabrication and Operation of Manganin Shock Pressure Gages," AFWL-TR-68-57, Air Force Weapons Laboratory, Aug 1968, pp. 75-79.

25. Barker, L. M., and Hollenbach, R. E., "Shock-Wave Studies of PMMA, Fused Silica, and Sapphire," Journal of Applied Physics, Vol. 41, No. 10, pp. 4208-4226.

26. Van Thiel, M.; Shanner, J.; and Sallinas, E., Compendium of Shock Wave Data, UCRL-108-Vol. 3, Lawerence Livermore National Laboratory, Livermore, CA, 1977, pp. 601-602.

27. Sutherland, G.T., private communication with N.S. Brar of Washington State University concerning the shear modulus of PMMA, Oct 1985.

REFERENCES (Cont.)

28. Gupta, Y. M., and Gupta, S. C., "Incorporation of strain hardening in piezoresistance analysis: Application to ytterbium foils in PMMA matrix," Journal of Applied Physics, Vol. 61, No. 2, 1987. [Note: Private communication with Y. M. Gupta (Sep 1988) revealed that the values given for the coefficients A and B on page 494 are a misprint; correct values should be 7.6 x 10^{-4} $kbar^{-2}$.]

29. Sutherland, G. T., unpublished Computer Code MATE, Naval Surface Warfare Center, 1987.

30. Tasker, D. G., and Lee, R. J., unpublished electrical schematic.

31. Tasker, D. G., unpublished drawing.

32. Gupta, S. C.; Gupta, Y. M.; and Williams M., "Piezoresistance Response of Ytterbium Foils in Shocked Liquid CS_2," in Shockwaves in Condensed Matter, edited by Schmidt, S. C., and Holmes, N. C., North-Holland, New York, NY, 1988.

33. McQueen, R. G., et al, "The Equation of State of Solids From Shock Wave Studies", High Velocity Impact Phenomena, Kinslow (ED.), Academic Press, New York, 1970, Chapter VII.

34. Sutherland, G.T., private conversation with M. Wong of Washington State University concerning anisotropy in ytterbium gauge foils, Sep 1988.

35. Sutherland, G.T., private communication with P. S. DeCarli of SRI International concerning the anisotropy in ytterbium gauge foils, Sep 1988.

36. Cagnoux, J., et al, Annales De Physique, Vol. 12, 1987, pp. 451-524.

37. Sutherland, G.T., private communication with Y. M. Gupta of Washington State University concerning the accuracies of ytterbium gauges, Sep 1988.

38. Erickson, et al, "Fabrication of Manganin Stress Gauges for Use in Detonating High Explosive" in Proceedings of the 10th Symposium on Explosives and Pyrotechnics, San Francisco, CA, 1979.

39. Graham, R. A.; Lee, L. M.; and Bauer, F.,"Response of Bauer Piezoelectric Polymer Stress Gauges (PVDF) to Shock Loading," in Shockwaves in Condensed Matter, edited by Schmidt, S. C., and Holmes, N. C., North-Holland, New York, NY, 1988.

40. Sutherland, G.T., private conversation with W. Wong of Washington State University concerning manganin gauge power supplies, Aug 1989.

41. Dobratz, B.M., and Crawford, P.C., LLNL Explosives Handbook, Properties of Chemical Explosives and Explosive Simulants, UCRL 52997, Change 2, 31 Jan 1985, LLNL, Livermore, CA.

42. Hall, T.N., and Holden, J.R., Navy Explosive Handbook Explosion Effects and Properties--Part III. Properties of Explosives and Explosive Compositions, NSWC MP 88-116, Oct 1988.

APPENDIX A

INCLUSION ANALYSIS FEATURES

The relative resistance change of a ytterbium gauge is related to the stresses and strains in the ytterbium[A-1] by Equation (A-1). Directions (see Figure A-1) are (1) along the width of gauge, (2) along gauge thickness, and (3) along the length of gauge.

$$\frac{\Delta R}{R_o} = \pi_{12}(\Delta\sigma_1 + \Delta\sigma_2) + \pi_{11}\Delta\sigma_3 + \eta\Delta\gamma_p - \Delta\epsilon_1 - \Delta\epsilon_2 + \Delta\epsilon_3 \qquad \text{(A-1)}$$

where:

ΔR = resistance change of gauge

R_0 = initial resistance of gauge

σ_i = stresses in the ytterbium gauge in kbar

ϵ_i = strains in the ytterbium gauge

γ_p = accumulated plastic strain in gauge

π_{1j} = piezoresistive coefficients

η = electrical strain hardening coefficient

The resistance of a ytterbium gauge is determined by three physical effects. The stress terms in Equation (A-1) model the resistance change that occurs when the ytterbium metal is stressed (piezoresistance). The strain terms model the resistance change caused by any dimensional change of the gauge. The term $\eta\Delta\gamma_p$ models the gauge resistance increase caused by defects produced in the ytterbium during plastic work on the gauge. These defects are produced during both plastic loading and unloading. The accumulated plastic strain (γ_p) is defined to be a scaler and will increase upon plastic loading and unloading.

To use Equation (A-1), the dependence of the stresses and strain (our shock experiments are one dimensional in strain) existing in the target material to the stresses and strains in the gauge needs to be determined. In this work, an inclusion analysis computer code[A-2] was used. For a given strain in the target material, the program calculates the stresses in the target material. The program also calculates the stresses, strains, and accumulated plastic strain in the ytterbium gauge. These

values are then inserted into Equation (A-1) to find the gauge resistance. This Appendix will describe how the inclusion analysis is used and some of its inherent limitations.

As described in earlier chapters, inclusion parameters are obtained from calibration experiments, assumption of material response, and quasi-static testing. A final matrix longitudinal strain is put into the computer code until a predicted gauge relative resistance change is obtained which is just slightly above the peak measured relative resistance change. A modified version of INCL51[A-2] generates a table of longitudinal matrix stress versus relative resistance change values for loading and unloading. Computer programs MATE or NMATE[A-3] are used to interpolate the above table and, for each measured relative resistance change, generate a corresponding stress for loading and unloading. The point where unloading is to occur is put into the program. This point is determined by visual inspection of the record.

In symmetric impact experiments in which the flyer is backed by a "vacuum," a slightly negative stress can result from the analysis. The true stress is zero. Variations in gauge material and the slight imprecision in gauge calibration can cause a measured relative resistance change corresponding to a negative stress. Negative stresses are found by extrapolating the slope of unloading stress versus relative resistance change values.

As mentioned before, the inclusion analysis is only strictly valid for an elastic matrix and an elastic-plastic gauge. By using some modifications, an elastic-plastic gauge in a hydrostatic matrix can be modeled. Unfortunately, the case in which an elastic-plastic gauge is placed in an elastic-plastic matrix cannot currently be modeled.

Materials in the inclusion analysis are treated as loading and unloading along the Raleigh line. This relationship is given by Equation (A-2). The above assumption is not correct for all unloading and unloading scenarios; it is discussed later in this appendix.

$$\sigma_l = (K + (4/3)\,\mu)\,\epsilon = L\,\epsilon \qquad \text{(A-2)}$$

where:

σ = longitudinal stress

K = bulk modulus

μ = shear modulus

L = longitudinal modulus

ϵ = longitudinal strain

To illustrate the limitations of the inclusion analysis, consider finding stress-time points from an arbitrary relative resistance change-time profile like that represented by Figure A-2. This profile is fictious: no real material would generate such a profile. The first three steps denoted by region (A) represent a triple shock. A release in the form of a rarefaction shock leading to complete unloading

is represented by (B). Region (C) represents the relative resistance change corresponding to zero stress. A ramp wave which represents recompression is denoted by (D). A complete unloading by means of rarefaction is denoted by (E). Region (F) represents the relative resistance change corresponding to zero stress.

Region (A) denotes a triple shock; the material will load in stress-strain space by means of three Raleigh lines. The present inclusion analysis can only consider loading along one Raleigh line. One could either calculate the stress of the first step or consider a Raleigh line for a single shock of stress amplitude equal to that of the material after being shocked by the three shocks. This assumption will lead to errors in calculating pressure. This error will become greater for higher strains and will also be greater for materials whose Hugoniot have large curvature or have a large Gruneisen constant (Γ).[A-4] A specialized inclusion analysis was written by Gupta and Gupta[A-5] to analyze double shock experiments.

Region (B) denotes a rarefaction shock. The present inclusion analysis program treats unloading as occurring along the Raleigh line. In the case of a rarefaction shock, unloading does occur along the Raleigh line.

Region (C) denotes the relative resistance change measured when the material is unloaded. It is non-zero because of residual strains in the ytterbium gauge, and defects were generated in ytterbium.

Region (D) denotes a ramp wave compression. Material compressed by means of a ramp wave are quasi-isentropic. This means that loading will not occur along a Raleigh line. An inclusion analysis will also have to take into account the initial non-zero relative resistance change. The inclusion analysis currently used cannot handle a case of recompression. Brar and Gupta[A-6] have investigated the effect of ramp wave loading (in compression-release experiments using fused silica) and concluded that the analysis will accurately predict peak pressures. The non-Raleigh line loading will result in a false value of stress to be predicted at strains between the initial and final strains. Wong[A-7] recently wrote a routine for the inclusion analysis program which will model the loading response of fused silica.

Region (E) denotes an unloading caused by a rarefaction wave. In real materials, a rarefaction shock would not occur after a material has been loaded by a ramp wave. A rarefaction unloads almost isentropically. The inclusion analysis treats loading as occurring down the Raleigh line. This means that false values of stress are predicted at strains between the initial and final strains.

Region (F) denotes the relative resistance change corresponding to unloading of the material.

It is recommended that an inclusion analysis be developed to treat the case of an elastic-plastic gauge in an elastic-plastic matrix. In addition, it is recommended that an inclusion analysis be developed to treat arbitrary waveforms. This analysis could incorporate a Mie-Gruneisen equation of state and the user would indicate which regions are loaded or unloaded along either a Raleigh line or a isentrope. In the case of a double shocked material, the user would tell the analysis which part of the record corresponded to the first shock and which to the second shock.

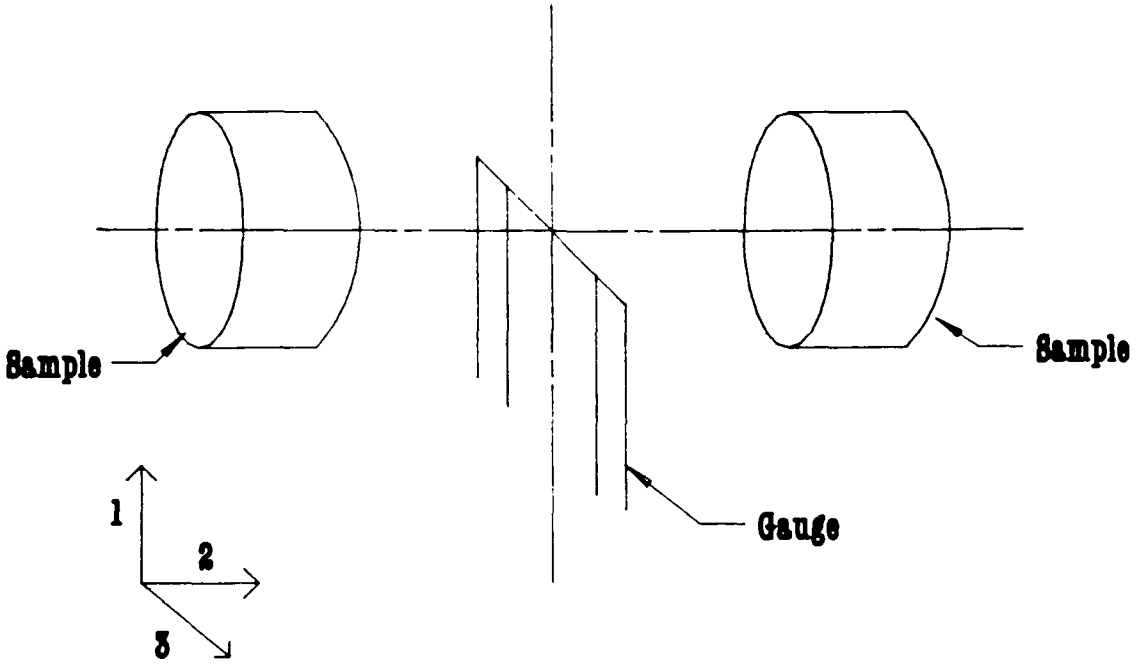

NOTE: DIRECTIONS ARE: (1) ALONG WIDTH OF GAUGE, (2) ALONG THICKNESS OF GAUGE, AND (3) ALONG LENGTH OF GAUGE.

FIGURE A-1 EXPLODED VIEW OF AN INSITU GAUGE

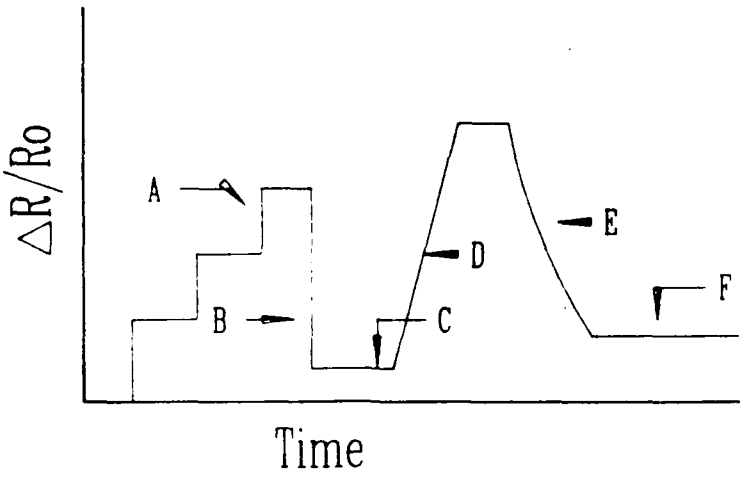

FIGURE A-2 ARBITRARY RELATIVE RESISTANCE CHANGE-TIME PROFILE

APPENDIX A

REFERENCES

A-1. Gupta, S. C. and Gupta, Y. M., "Piezoresistance response of longitudinally and laterally oriented ytterbium foils subjected to impact and quasi-static loading." Journal of Applied Physics, Vol. 57, No. 7, 1985, pp. 2464-2472.

A-2. Gupta, Y. M.; Gupta, S. C; and Wong, M., unpublished Computer Code INCL51, Washington State University, 1987.

A-3. Sutherland, G. T., unpublished Computer Codes MATE and NMATE, Naval Surface Warfare Center, 1987.

A-4. Grady, D., "Shock Induced Magnetic Anisotropy in Yttrium Iron Garnet", Ph.D dissertation, Washington State University, 1971, pp. 58-60.

A-5. Sutherland, G.T., private communication with M. Wong of Washington State University concerning a two step inclusion analysis, 1 Sep 1988.

A-6. Brar, N. S., and Gupta, Y. M., "Piezoresistance response of ytterbium foil gauges shocked to 45 kbar in fused silica matrix," Journal of Applied Physics, Vol. 61, No. 4, 1987.

A-7. Sutherland, G.T., private communication with M. Wong of Washington State University concerning alterations to the INCL 51 computer code, 1 Sep 1988.

APPENDIX B

RESOLUTION OF NICOLET DIGITIZERS

In some experiments, a Model 2090 Nicolet digitizer was used with a Model 205A 50 Mhtz plug in. The single shot digitizing rate was 20 nsec per data point. A Nicolet digitizer allows for direct transfer of experimental data into a Compaq Deskpro 286 Computer.

Resolution of the Nicolet digitizer is 8 bits; the voltage range is divided into 256 divisions. For example, if a voltage range of ± 400 millivolts was selected, a resolution of about 0.0031 volts is obtained. The uncertainty in voltage will then be about ± 0.0015 volts. The digitizing rate of the Nicolet unit was 20 nsec per point; each point is known to ± 10 nsec.

The experimental resolution obtained is intentionally less than the maximum resolution afforded by the digitizer. Figure B-1 shows a schematic representation of an arbitrary voltage-time record taken during a ytterbium gauge experiment. To make sure that all the record is displayed, the voltage corresponding to point B is typically 50 to 70 percent of the maximum voltage. The zero voltage line is also typically offset from the bottom by a small voltage offset.

For the sake of argument, let the voltage denoted by dimension A be 100 divisions, the voltage denoted by dimension B be 150 divisions, and the voltage denoted by dimension C be 104 divisions. The initial voltage (A) is the voltage drop measured across the gauge element before the gauge is shocked (initial resistance times the current). The voltage given by (B) is the voltage drop due to the increased resistance of the gauge when it is shocked. When the gauge is unloaded, the resistance of the gauge will be higher than initially and the voltage drop that is measured will be denoted by (C). What needs to be obtained is the relative voltage change, $\Delta V/V_o$. This measurement will be converted through the use of a circuit equation into a relative resistance change, $\Delta R/R_o$. The relative resistance change is typically within a few percent of the relative voltage change.

Assuming the zero line to be truly zero, the relative voltage change denoted by dimension B is (50 ± .5)/(100 ± .5). The relative voltage change denoted by dimension C is (8 ± .5)/(100 ± .5). From an error analysis following Beers[B-1] this gives a relative voltage drop of 0.500 ± .005 for (B) and 0.08 ± .005 for (C). This corresponds to a ± 1 percent uncertainty for (B) and a ± 6 percent uncertainty for (A). This uncertainty is reflected in the coarseness of some of the experimental records taken with a Nicolet digitizer (see Figures B-2 and B-3). The measurement of the residual relative voltage change (C) is used in calibration experiments to obtain the constant η. A small change in the measured residual relative voltage change can result in large changes in the obtained value for η.

Tasker[B-2] suggested that a bridge circuit be constructed to subtract the initial voltage drop. He suggested measuring the initial voltage drop with a slower 12-bit digitizer. The resulting signal could

then be measured with an 8-bit Nicolet digitizer. The relative voltage change would be measured as 0.500 ± 0.0025 for (B), and a relative voltage drop of 0.08 ± .0313 for (C). This corresponds to a ± .5 percent uncertainty for (B) and a ± 3 percent uncertainty for (B). A digitizer or oscilloscope could be configured to measure just the residual relative voltage change if more accuracy was needed.

A 4-channel digitizer with a sampling speed of 5 nsec per point would allow the acquisition of 4 time-correlated records. The finer time resolution of this digitizer would allow for more accurate shock velocity measurements.

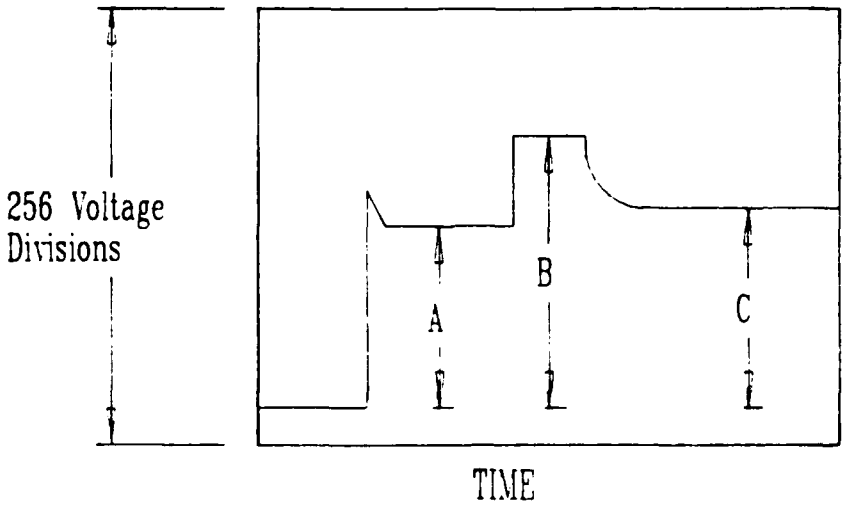

FIGURE B-1. SCHEMATIC REPRESENTATION OF VOLTAGE DROP OBSERVED FOR A YTTERBIUM GAUGE CALIBRATION COMPRESSION-RELEASE EXPERIMENT

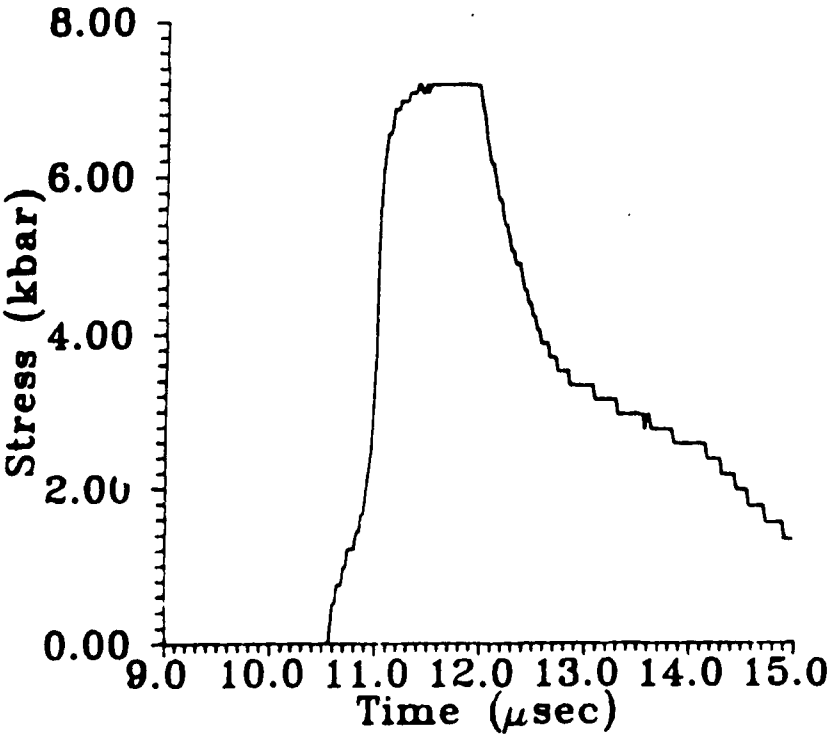

FIGURE B-2 EXPERIMENTAL STRESS-TIME PROFILE OBTAINED WITH THE USE OF A NICOLET DIGITIZER FOR EXPERIMENT 87-008

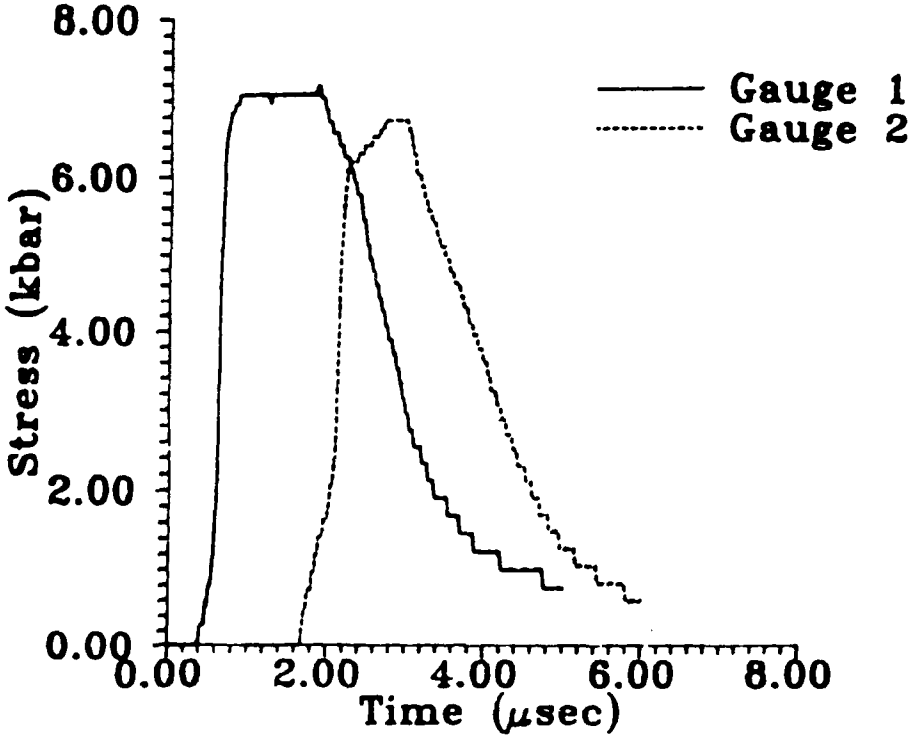

FIGURE B-3. EXPERIMENTAL STRESS-TIME PROFILE OBTAINED WITH THE USE OF A NICOLET DIGITIZER FOR EXPERIMENT 87-009

APPENDIX B

REFERENCES

B-1. Beers, Y., Introduction to the Theory of Errors, Addison-Wesley Publishing Co., Inc., Reading, MA, 1957.

B-2. Sutherland, G.T., private communication with Doug Tasker of Naval Surface Warfare Center concerning bridge circuits, Aug 1988.

APPENDIX C

WONDY HYDROCODE CALCULATIONS

Composition B-3 experiments were modeled using the WONDY Hydrocode.[C-1] This code was run on a CDC 865 mainframe computer located at NSWC (Dahlgren, VA). The equation of state (EOS) used to model Composition B-3 and fused silica was a Mie-Gruneisen EOS. This is written mathematically as Equation (C-1). Units will be given in shock units (megabar, gr/cc, etc.) for the convenience of computational shock physicists.

$$P(V,E) = P_H(V) - (\Gamma/V)(E - E_H) \qquad \text{(C-1)}$$

where:

E_H = energy along a Hugoniot
P_H = pressure along a *Hugoniot*
V = volume
E = energy along an EOS surface
P = pressure along an EOS surface
Γ = Gruneisen constant

On the Hugoniot $E = E_H$, meaning the second term on the right hand side of Equation (C-1) is zero. The Gruneisen constant allows for the calculation of p-v paths for unloading, ramp wave loading, and multi-shock loading, or when material response cannot be determined by a single Hugoniot.

Material parameters for Fused Silica and Composition B-3 are found in Table C-1. The models that use these parameters are described below.

Fused Silica was modeled using a stress-strain relationship of Barker and Hollenback.[C-2] The WONDY hydrocode requires that stress-strain relationships be in the form of Equation (C-2).[C-1]

$$P_H = K_o\epsilon(1 + K1\epsilon + K_2\epsilon^2 + K_3\epsilon^3 + ...) \quad (C\text{-}2)$$

where:

ϵ = strain

$K_o = \rho_o C_o^2$ = adiabatic bulk modulus

C_o = bulk sound speed in cm μsec^{-1}

ρ_o = density in gr cm^{-3}

For Composition B-3, a linear shock velocity-particle velocity relationship was input into the code. Fused silica was modeled as being hydrostatic, and Composition B-3 was modeled as being elastic-plastic. Composition B-3 was taken to yield (not the HEL) at 0.00058 megabar.

$$U = C_o + A\,u_p \quad (C\text{-}3)$$

where:

C_o = bulk sound speed in cm μsec^{-1}

A = Hugoniot curvature

U = shock velocity in cm usec^{-1}

u_p = shock velocity in cm usec^{-1}

TABLE. C-1. WONDY CODE INPUT PARAMETERS

Material	Bulk Sound Speed (cm μsec^{-1})	Density (g cm^{-3})	Hugoniot Curvature (A)	K_1	K_2	K_3	Gruneisen Constant (Γ)	Poisson's Ratio (ν)
Comp B-3	0.2216	1.71	2.466	------	-------	------	1.0	0.295
Fused Silica	0.593	2.201	------	-5.3595	39.0979	-89.2526	3.0	-----

APPENDIX C

REFERENCES

C-1. Kipp, M. E., and Lawrence, R. J., WONDY V - A One-Dimensional Finite-Difference Wave Propagation Code, SANDI81-0930, Sandia National Laboratories, Jun 1982.

C-2. Barker, L. M., and Hollenbach, R. E., "Shock Wave Studies of PMMA, Fused Silica and Sapphire," Journal of Applied Physics, Vol. 41, No. 10, 1970.

APPENDIX D

EULERIAN RELEASE VELOCITY AS MEASURED FROM MULTIPLE INSITU GAUGES

In this appendix, a derivation suggested by Gupta[D-1] is presented in which the relationship between Lagrangian sound speed (C_l) upon release, and Eulerian sound speed (C_e) upon release is obtained.

The ratio of differential increments in Lagrangian and Eulerian displacement is given by

$$\frac{dx}{dh} = \frac{\rho_o}{\rho} \tag{D-1}$$

where x is the Eulerian displacement, h is the Lagrangian displacement, ρ_o is the density of the unshocked material, and ρ is the density of the shocked material. The total differential of the Eulerian displacement as a function of Lagrangian displacement and time is given by

$$dx = \frac{\partial x}{\partial h} dh + \frac{\partial x}{\partial t} dt \tag{D-2}$$

Note that particle velocity is by definition $\partial x/\partial t$. The above equation, when divided by the differential gives dt,

$$\frac{dx}{dt} = \frac{\partial x}{\partial h}\frac{dh}{dt} + u_p. \tag{D-3}$$

The disturbance velocity (dx/dt) of the release is $C_e + u_p$; this gives

$$C_e + u_p = \frac{\partial x}{\partial h}\frac{dh}{dt} + u_p. \tag{D-4}$$

The concept of a disturbance velocity can be thought of as the following. Imagine that you are looking at a release wave propagating through a material. Divide the release wave into infinitesimal shocklets (see Figure D-1). Each shocklet has associated with it a unique velocity. We will consider the velocity of shocklet 1 in Figure D-1. Any disturbance propagating into the shock will be swept along with the flow. This flow will be travelling at a speed given by the particle velocity. Hence, the first shocklet will travel at a speed (disturbance velocity) which is the particle velocity plus the

sound speed.

Equation (D-1) means that Equation (D-4) becomes

$$C_e = \frac{\rho_o}{\rho}\frac{dh}{dt} = \frac{\rho_o}{\rho} C_l. \qquad \text{(D-5)}$$

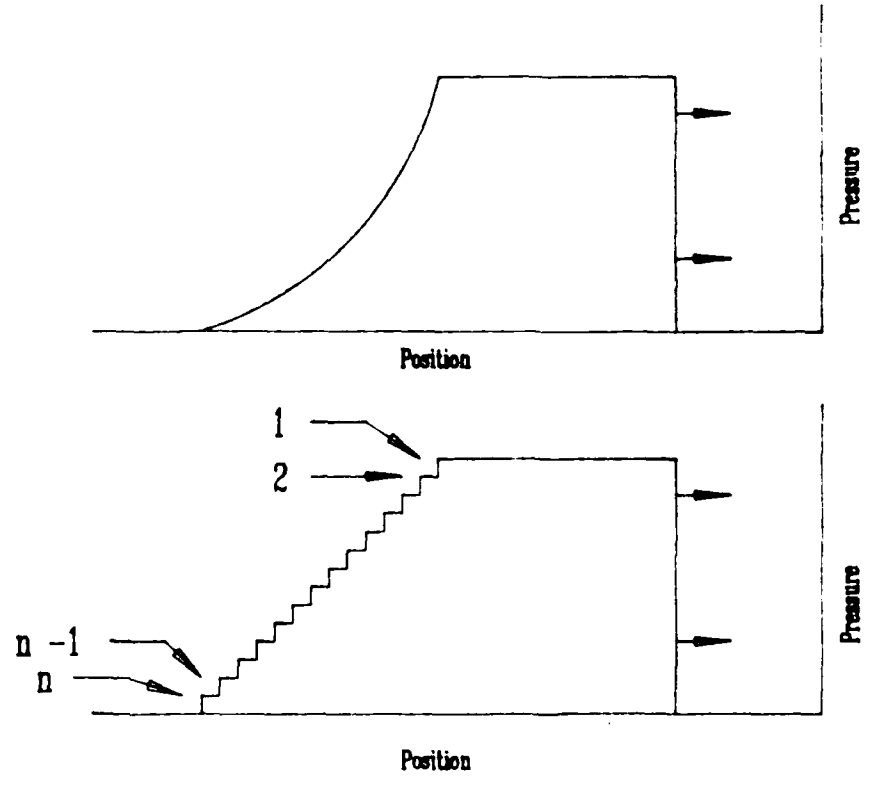

NOTE: AS THE NUMBER OF SHOCKLETS GETS VERY LARGE THE RELEASE PROFILES SHOWN ABOVE WILL BECOME IDENTICAL.

FIGURE D-1 THE REPRESENTATION OF MODELING A RELEASE WAVE AS A SERIES OF SHOCKLETS

APPENDIX D

REFERENCES

D-1. Forbes, J. W., private communication with Y. M. Gupta of Washington State University concerning method of calculating sound speed on release, 1 Aug 1988.

DISTRIBUTION

	Copies
Office of the Chief of Naval Research	
Attn: ONR 1132P (R. Miller)	1
ONR 123 (A. Roberts)	1
ONT 21 (E. Zimet)	1
ONT 213 (D. Siegel)	1
ONT 23 (A. Faulstich)	1
ONT 232 (D. Houser)	1
800 N. Quincy Street, BCT 1	
Arlington, VA 22217-5000	
Commander	
Naval Sea Systems Command	
Attn: SEA-03A31	2
SEA-662	1
SEA-6622	1
Washington, DC 20362-5105	
Commander	
Naval Air Systems Command	
Attn: AIR-932	1
AIR-932F	1
AIR-932H	1
AIR-932T	1
Washington, DC 20361	
Naval Ordnance Station	
Attn: Code 2730D	1
Technical Library	1
Indian Head, MD 20640-5000	
Commanding Officer	
Naval Weapons Station	
Attn: Code 470A (L. Leonard)	1
Library	1
Yorktown, VA 23691-5000	
Superintendent	
Naval Postgraduate School	
Attn: Library	1
Monterey, CA 93940	

	Copies
Commander	
Space and Naval Warfare Systems Command	
Attn: SPAWAR-05	1
Washington, DC 20363-5100	
Commander	
Naval Weapons Center	
Attn: Code 38 (R. Derr)	1
Code 389 (T. Boggs)	1
Code 32	1
Code 326	1
Code 326B (G. Greene)	1
Code 326B (L. Josephson)	1
Code 3261	1
Code 3266 (D. Lind)	1
Code 3265	1
Code 3265 (J. Pakulak)	1
Code 385	1
Code 3853 (R. Hollins)	1
Code 3853 (R. Yee)	1
Code 3891 (M. Chan)	1
Code 3891 (H. Richter)	1
Code 39	1
China Lake, CA 93555	
Commander	
Naval Research Laboratory	
Attn: Technical Information	1
Washington, DC 20375	
Commander	
Naval Intelligence Support Center	
Attn: NISC-30	1
NISC-60, Library	1
LNN, Liaison Office	1
4301 Suitland Road	
Washington, DC 20340	
David Taylor Research Center	
Attn: Technical Library	1
R. Garrison	1
Bethesda, MD 20084	

DISTRIBUTION (Cont.)

	Copies
Marine Corps Development and Education Command	
Attn: Library	1
Marine Corps Landing Force Development Center	
Quantico, VA 22134	
Commander	
U.S. Army Laboratory Command	
Attn: AMSLC-TD (Vitali)	1
2800 Powder Mill Road	
Adelphi, MD 20783	
Commanding Officer	
Harry Diamond Laboratories	
Attn: DELHD-DE-OM (Warner)	1
Library	1
2800 Powder Mill Road	
Adelphi, MD 20738	
Army Armament Research and Development Command	
Attn: DRSMC-LCE	1
DRSMC-LCE-C	1
DRSMC-LCE-D	2
Dover, NJ 07801	
Commanding Officer	
Ballistic Research Laboratory	
USARRADCOM	
Attn: Technical Library	1
P. Howe	1
STINFO Office	1
V. Boyle	1
R. Frey	1
R. Jamieson	1
J. Starkenberg	1
J. Watson	1
Aberdeen Proving Ground, MD 21005	

	Copies
Army Materials and Mechanics Research Center	
Attn: D. Dandekar	1
Watertown, MA 02172	
Air Force Armament Division	
Attn: AFATL/MNE	1
AFATL/MNW	1
AFATL/DLODL	1
Eglin Air Force Base, FL 32542-6009	
Defense Technical Information Center	
Cameron Station	
Alexandria, VA 22304-6145	12
Department of Defense Explosives Safety Board	
Attn: 6-A-145	1
J.Ward	1
Hoffman Building 1	
2461 Eisenhower Avenue	
Alexandria, VA 22331	
Library of Congress	
Attn: Gift and Exchange Division	4
Washington, DC 20540	
Department of Commerce	
Patent and Trademark Office	
Group 130, Bldg 3	
Attn: M. Savage	1
Washington, DC 20231	
Los Alamos National Laboratory	
Attn: M-6 (J. Shaner)	1
M-9 (J. Dick)	1
M-9 (S. Sheffield)	1
M-9 (R. Rabie)	1
M-9 (J. Wackerle)	1
P.O. Box 1663	
Los Alamos, NM 87545	

DISTRIBUTION (Cont.)

	Copies
Sandia National Laboratories	
Attn: D. E. Grady	1
R. A. Graham	1
J. R. Asay	1
L. C. Chhabildas	1
J. Wise	1
Thermomechanical & Physical Division	
Albuquerque, NM 87185-5800	
University of California	
Lawrence Livermore National Laboratory	
Attn: E. L. Lee	1
D. B. Larson	1
R. L. Simpson	1
R. B. Stout	1
P. A. Urtiew	1
L. M. Erickson	1
R. C. Weingart	1
A. C. Mitchell	1
W. J. Nellis	1
E. J. Nidick	1
P.O. Box 808	
Livermore, CA 94550	
Washington State University	
Department of Physics	
Shock Dynamics Laboratory	
Attn: Y. M. Gupta	1
G. E. Duvall	1
M. Wong	2
R. Gustavson	1
P. Bellamy	1
T. Schilling	1
Pullman, WA 99164	
University of Dayton Research Institute	
Impact Physics Facility, KLA 14	
Attn: N. Brar	1
Z. Rosenberg	1
S. Bless	1
300 College Park	
Dayton, OH 45469	

	Copies
University of Maryland	
Department of Mechanical Engineering	
Attn: R. Armstrong	1
R. Dick	1
College Park, MD 20742	
ATR	
Attn: W. Watt	1
S. Jacobs	1
D. Price	1
14900 Sweitzer Lane	
Laurel, MD 20707	
SRI International	
Attn: Document Center	1
M. Cowperthwaithe	1
S. Miller	1
D. Keough	1
P. DeCarli	1
333 Ravenswood Avenue	
Menlo Park, CA 94025	
Ireco Incorporated	
Attn: R. Granholm	1
3000W 8600S	
West Jordan, UT 84088	
Hercules Aerospace Company	
Attn: M. Klakken	1
Bacchus Works	
Magna, UT 84044-0098	
Southwest Research Institute	
Attn: C. Anderson	1
San Antonio, TX 78284	
British Embassy	
Attn: A. Robinson	1
British Defense Staff	
3100 Massachusetts Ave., N. W.	
Washington, DC 20008	

DISTRIBUTION (Cont.)

	Copies
Royal Ordnance Ammunition	
Attn: P. R. Lee	1
Buxton Lane	
Buxton, Chorley, Lancaster	
PR7, 6AD United Kingdom	
Atomic Weapons Establishment	
Attn: C. Beck	1
G. Eden	1
G. Foan	1
D. Grief	1
C. Hutchinson	1
Aldermaston, Reading	
Berkshire, RG7 4PR, United Kingdom	
Atomic Weapons Establishment	
Attn: H. James	1
Foulness Island, Southend-on-Sea	
Essex, United Kingdom	
Royal Armament Research and	
Development Establishment	
Attn: J. Connor	1
I. Cullis	1
P. Haskins	1
M. Nash	1
Fort Halstead	
Sevenoaks, Kent, United Kingdom	
Royal Armament Research and	
Development Establishment	
Attn: K. Bascombe	1
J. Jenkins	1
G. Hooper	1
D. Mullenger	1
B. Hammant	1
A. Kosecki	1
Waltham Abbey, Powdermill Lane	
Essex EN9 1BP, United Kingdom	

	Copies
Centre d'Etudes	
Attn: P. Chartagnac	1
M. Perez	1
Bedes 46500	
Gramat, France	
Materials Research Laboratories	
Attn: G. Yiannakopoules	1
D. Richardson	1
P.O. Box 50, Ascot Vale	
Melbourne, Victoria 3032	
Australia	
Satish Gupta	1
Neutron Physics Division	
Bhabha Atomic Research Centre	
Bombay 400085	
India	

DISTRIBUTION (Cont.)

		Copies
Internal Distribution:		
E231		2
E232		15
E35	(GIDEP Office)	1
G22	(W. Holt)	1
	(W. Mock)	1
	(S. Wagner)	1
	(W. Soper)	1
R		1
R04		1
R10		1
R101		1
R10A	(D. Phillips)	1
R10A	(K. Reed)	1
R10B		1
R10C		2
R10D		1
R10E		1
R10F		1
R10G		1
R101		1
R11		1
R11	(E. Anderson)	1
	(R. Doherty)	1
	(C. Gotzmer)	1
	(V. Ringbloom)	1
R12		1
R12	(K. Carlson)	1
	(P. Spahn)	1
	(P. Walter)	1
R13		1
R13	(D. Ashwell)	1
	(R. Baker)	1
	(R. Bardo)	1
	(A. Brown)	1
	(R. Clairmont)	1
	(S. Coffey)	1
	(J. Davis)	1
	(D. Demske)	1
	(J. Forbes)	3
	(B. Glancy)	1

		Copies
Internal Distribution (Cont.):		
R13 (Cont.):		
	(C. Groves)	1
	(R. Gurrguis)	1
	(P. Gustavson)	1
	(H. Jones)	1
	(R. Lee)	1
	(W. Lee)	1
	(R. Lemar)	1
	(P. Miller)	1
	(C. Richmond)	1
	(H. Sandusky)	1
	(G. Sutherland)	10
	(D. Tasker)	1
	(W. Wilson)	1
	(D. Woody)	1
	(F. Zerilli)	1
R14		1
R14	(D. Lehto)	1
R15		1
	(M. Swisdak)	1
	(R. Tussing)	1
R16		1
U12	(W. Walker)	1
E22		1